Structure and functionality of polyelectrolyte brushes, a surface force perspective

Xin Xu[1,2]†, Mark Billing[3]†, Marina Ruths[2], Harm-Anton Klok[1,3], Jing Yu[1*]

1 School of Materials Science and Engineering, Nanyang Technological University, Singapore 639798.

2 Department of Chemistry, University of Massachusetts Lowell, Lowell, MA 01854, USA.

3 Institut des Matériaux et Institut des Sciences et Ingénierie Chimiques, Laboratoire des Polymères, École Polytechnique Fédérale de Lausanne (EPFL), Bâtiment MXD, Station 12, CH-1015 Lausanne, Switzerland.

***** yujing@ntu.edu.sg

†These authors contributed equally to this work.

Abstract

The unique functionalities of polyelectrolyte brushes depend on several types of specific interactions, including solvent structure effects, hydrophobic forces, electrostatic interactions, and specific ion interactions. Subtle variations in the solution environment can lead to conformational and surface structural changes of the polyelectrolyte brushes, which is discussed mainly from a surface interaction perspective in this review. A brief overview is given of recent theoretical and experimental progress on the structure of polyelectrolyte brushes in various environments. Two important techniques for surface force measurements are described, the Surface Forces Apparatus (SFA) and the Atomic Force Microscope (AFM), and some recent results on polyelectrolyte brushes are shown. Lastly, this review highlights the use of these surface-grafted polymer films to create functional surfaces for various applications, including non-fouling surfaces, boundary lubricants, as well as stimuli-responsive surfaces.

1. Introduction

Polyelectrolyte brushes have drawn wide interest over decades owing to their unique properties. A brush structure is formed when polymer chains are anchored to a surface at high tethering densities.[1] Attaching the chain ends to a surface effectively fixes the characteristic length between polymer chains, which leads to behaviors not found for free chains: polyelectrolyte chains in the brush configuration are always stretched in contrast to their isolated coil state in solution (Fig. 1a).[2] This unique structure of polymer brushes has an impact on many important properties such as steric stabilization of colloidal systems and lubrication.[3] With the advance of surface-initiated polymerization techniques for making well-controlled brush systems, the interest in polyelectrolyte brushes has greatly expanded into the realm of functional surfaces with a broad spectrum of applications, such as antifouling, controlling wettability, adhesion, and lubrication of surfaces[3c, 4], regulating transport of ions and molecules[5], or converting chemical and biochemical stimuli into optical[6], electrical[7], chemical[8], and mechanical signals[9].

Much of the original interest in polyelectrolyte brushes is due to the lubricity of polyelectrolyte brushes, which are common in biological lubrication systems, such as in articular joints.[10] On the cartilage surface, some biomacromolecules, such as hyaluronic acid and lubricin, form brush like structures, which provide effective boundary lubrication with a friction coefficient as low as 0.001, preventing wear of the cartilage.[10a] Such excellent lubricity has also been observed in various synthetic polyelectrolyte brush systems.[3d, 4b, 11] The unique properties of these systems mainly come from the extended structure of the polyelectrolyte chains, resulting from a combination of long range electrostatic and short range steric interactions. Because of the charged nature of the polyelectrolyte chains, the degree of chain stretching, or the height of the brush, is highly sensitive to the surrounding solution environment, including the pH, ionic strength, salts, and solvent quality. Due to their tunable nature, there is also a growing interest in using polyelectrolyte brushes as responsive materials.[12]

An important class of polyelectrolytes includes weakly dissociating polyacids and polybases. Such polyelectrolytes form weak (or annealed) polyelectrolyte brushes. The degree of ionization of a weak polyelectrolyte is a function of the solution pH and salt concentration, and a non-monotonic behavior is observed in both experiments and theory.[13] The science behind this is still not well-understood, and has attracted the attention of many research groups. This review, however, will focus on brushes formed by strong (so-called quenched) polyelectrolytes, in which the number and positions of the charges are fixed, and theory is better established.[2, 14] However, as we shall elaborate in the rest of this review, the understanding of strong polyelectrolyte brushes is also still incomplete, and awaits further investigations. In the rest of the paper, the term polyelectrolyte brushes will be used to refer to strong polyelectrolyte brushes. The remainder of this review is subdivided in 6 sections. First, we will briefly review the theory on polyelectrolyte brushes. After that, the insights obtained on the structure and properties of polyelectrolyte brushes using surface forces apparatus (SFA) and atomic force microscopy (AFM) experiments will be discussed. The final three sections will focus on polyelectrolyte brushes prepared via surface-initiated polymerization and will successively present the use of these surface-grafted polymer films as non-fouling surfaces and boundary lubricants as well as describe their stimuli-responsive properties.

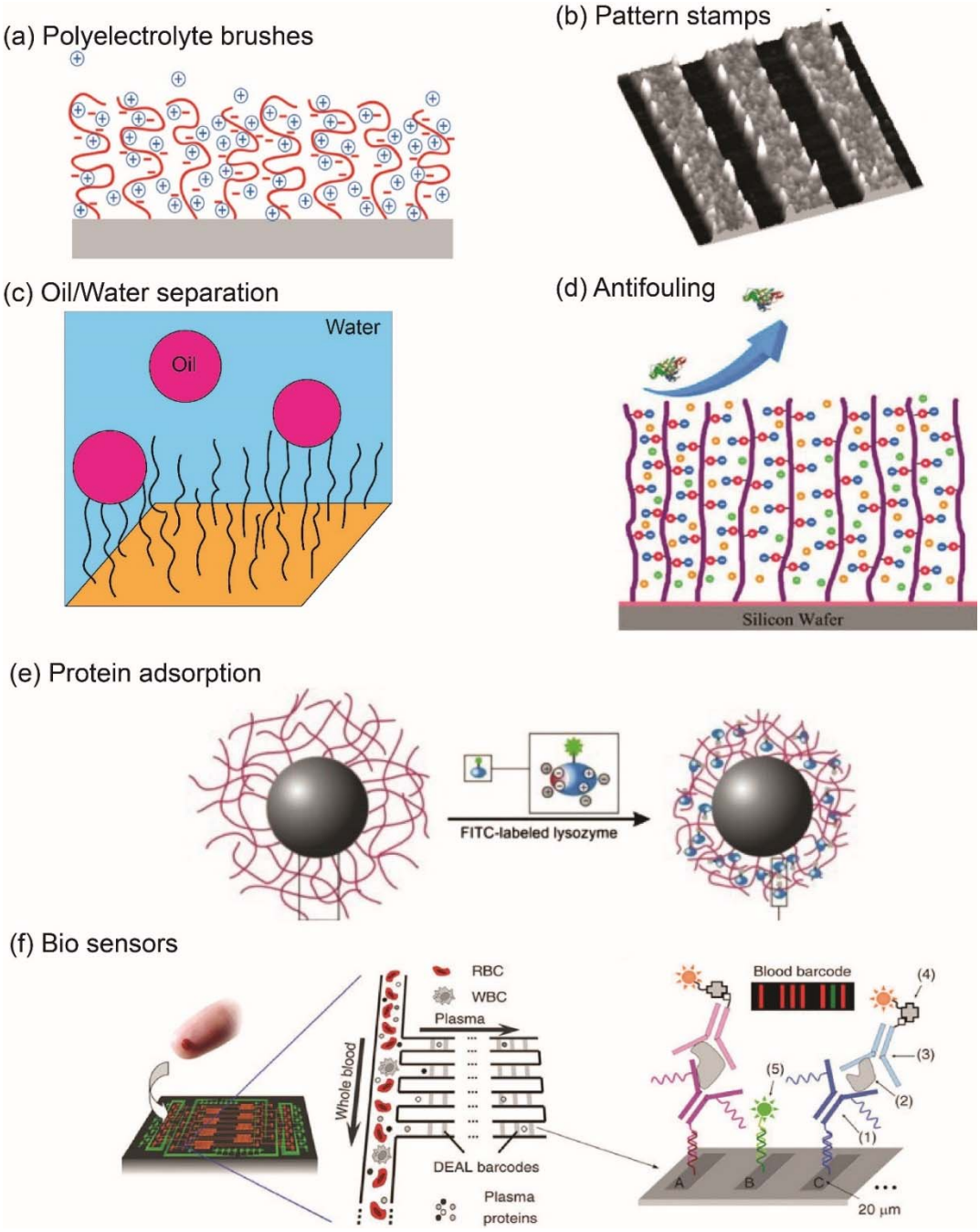

Figure 1. Illustrations of polyelectrolyte brushes and applications. a) Schematic of polyelectrolyte brushes. b) Polyelectrolyte brushes as ink reservoirs for pattern stamps. Reproduced from Ref.[15] with permission. c) Polyzwitterion brush grafted membrane for oil/water separation. Reproduced from Ref.[16] with permission from the Royal Society of Chemistry. d) Polyelectrolyte brush with antifouling property. Reprinted and adapted with permission from Ref.[17]. Copyright (2015) American Chemical Society. e) Polyelectrolyte brush grafted nanoparticles using for protein adsorptions. Reprinted and adapted with permission from Ref.[5a]. f) DNA brush chip for protein analysis using microliter quantities of blood. Reprinted and adapted with permission from Ref.[6].

2. Theory of Polyelectrolyte Brushes

For neutral polymer brushes, the dense assembly requirement is met when the average grafting distance between two neighbouring chains is smaller than the radius of gyration R_g of the polymer chain.[1a, 18] For a polymer with a degree of polymerization N,

$$R_g \propto N^{\nu}, \tag{1}$$

where the exponent ν for flexible macromolecules depends on the solvent quality ranging from 1/3 for a poor solvent to 1/2 for a θ-solvent to 3/5 for a good solvent.[19] The overlap density is defined as $\sigma_0 = N/\pi R_g^2$.

If the grafting density σ is greater than the overlap density, steric interactions between the polymer chains force the macromolecules into a stretched, extended conformation to relieve local crowding. The extension of a polymer brush is determined by a balance between the osmotic pressure Π arising from contacts between the polymer segments and the entropic elasticity opposing the stretching of the polymer chains.[1a, 20] For a brush in a good solvent, its thickness can be expressed as[21]

$$H \propto N\sigma^{\alpha}, \tag{2}$$

where σ is the grafting density, and the exponent α is related to ν through

$$\alpha = \frac{1}{2(\frac{1}{\nu}-1)}. \tag{3}$$

The charges of the polyelectrolyte chains bring another level of complexity to the brush system due to not only the long-range electrostatic interactions between charges but also the counterions in solution.[2, 14b, 22] In solution, the charge of the polyelectrolyte is always compensated by oppositely charged ions, or so-called counterions. The distribution of the counterions introduces another length scale, the Debye screening length κ^{-1}, into the system.[2] The structure and properties of polyelectrolyte brushes therefore are dramatically influenced by the surrounding environment, e.g., ionic strength, pH, and counterions.

Despite the complexity of the coupling of short-range steric and long-range electrostatic interactions in polyelectrolyte brush systems, scaling and self-consistent field theories incorporating Poisson–Boltzmann equations show that, under most conditions, nearly all the counterions compensating the charge of the polymers are localized in the brush to minimize the free energy of the system, leading to an overall electroneutrality of a polyelectrolyte brush.[23] Such an electroneutrality plays a key role in the theory of polyelectrolyte brushes, as there are no unscreened electrostatic interactions longer-ranged than the correlation length.[2]

Pincus, and Zhulina and coworkers, were among the first to study strong polyelectrolyte brushes in solution using scaling theory, demonstrating that the height of polyelectrolyte brushes is mainly determined by a balance between the osmotic pressure of the counterions and the polyelectrolyte chain elasticity. [2, 14b] Two distinct regimes, the *osmotic brush* and *salted brush* regimes have been predicted by the scaling theory and validated experimentally.[2, 24] For relatively dense and strongly charged brushes in relatively low ionic strength, the thickness of the brushes is independent of the grafting density and solution ionic strength. This regime is called the *osmotic brush* regime. In the *osmotic brush* regime, the thickness of the brush in a θ-solvent is given by

$$H \sim N f^{0.5}, \tag{4}$$

where f is the fraction of charged monomers.[2] At higher salt concentration, the brushes enter the so-called *salted brush* regime, in which the thickness of the brushes follows,

$$h \sim N f^{2/3} \sigma^{1/3} C_s^{-1/3}, \quad (5)$$

where C_s is the solution salt concentration.

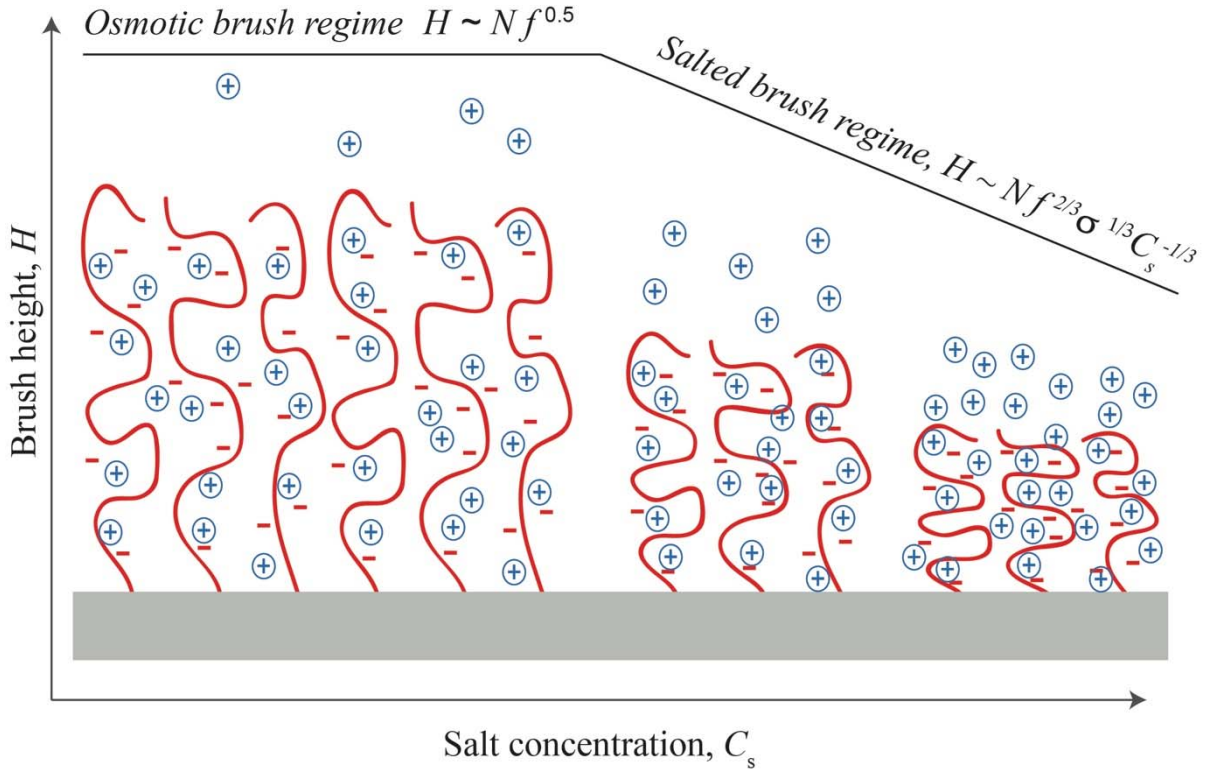

Figure 2. Change of the brush thickness in the osmotic brush and salted brush regimes predicted by scaling theory.

The transition from the *osmotic brush* to the *salted brush* regime has been confirmed experimentally. Guenoun et al. studied free-standing poly(*t*-butyl styrene)-*b*-poly(styrene sulfonate) (PtBS-*b*-PSS) diblock polymer films at the air–water interface with X-ray reflectivity technique.[25] Their results showed that the thickness of a PSS brush did not decrease with the addition of NaCl salt below a threshold of 0.1 M, but decreased with a −1/3 power law above the 0.1 M threshold. Several subsequent studies have also confirmed the transition of the osmotic to the salted brush regime in PSS brushes using various characterization techniques.[24b, c, 26] Scaling theory predicts that the crossover of the two regimes occurs when the solution salt concentration C_s equals the inner concentration of counterions C_I in the brush[2]; however, experimental results show that the transition from the *osmotic* to the *salted brush* regime required addition of only about 15–35% of C_I to the solution due to the phenomenon of counterion condensation.[22, 24b, 27] The condensed ions are not mobile and therefore are osmotically inactive. Experiments also show that the number of osmotically active counterions in the brush layer is lower than predicted by Manning condensation theory (64%).[27a] For example, Balastre et al. estimated that 80% counterions were condensed in physisorbed PtBS-PSS brushes via surface force measurements,[24b] and Ahrens *et al* found this percentage to be 90%. Such discrepancy between theory and experiments shows the complexity of polyelectrolyte brushes.[24c]

The existence of multivalent ions in solution can introduce dramatic structural changes to polyelectrolyte brushes. Such multivalent effects are very well-known experimentally but much less understood theoretically. Mei et al. reported a sharp decrease in brush height as a function of the valence and concentration of added multivalent ions using dynamic light scattering.[28] The rapid collapse of polyelectrolyte brushes induced by multivalent counterions has also been observed in SFA and neutron reflectivity measurements.[29]

Despite the success in explaining the structure and properties of polyelectrolyte brushes in monovalent salt solutions, the conventional approach of combining scaling theory and Poisson–Boltzmann equation still does not provide an adequate explanation of the multivalent effects due to strong ion condensation and charge correlation. Brettmann *et al.* provided an *ad hoc* theoretical model showing that the formation of lateral inhomogeneities in the collapsed polyelectrolyte brushes in the presence of multivalent counterions (Fig 3a). Molecular dynamics (MD) simulations have also shed light on the effects of multivalent counterions on the structure of polyelectrolyte brushes.[30] Liu et al. showed that the brush chains collapse heterogeneously into octopus-like surface micelles at a proper range of grafting density, polymer size, and ion concentration.[31] Jackson et al. demonstrated that while ostensibly forming similar micelle structures, solvophobic collapsed brushes and multivalent-ion collapsed brushes exhibit distinct mechanistic and structural features.[32] Yu et al., using a combination of AFM, SFA, and MD simulations, confirmed that solvophobic and multivalent-ion induced effects work in concert to drive strong phase separation of polyelectrolyte brushes, with electrostatic bridging of polyelectrolyte chains playing an essential role in the formation of the lateral structural inhomogeneities (Fig. 3b).[33] Considering the wide existence of multivalent ions in biological systems and industrial formulations, an understanding of these effects is particularly relevant for the interaction of polyelectrolyte brushes with multivalent charged materials such as proteins, nanoparticles, and oppositely charged polyelectrolytes.[34]

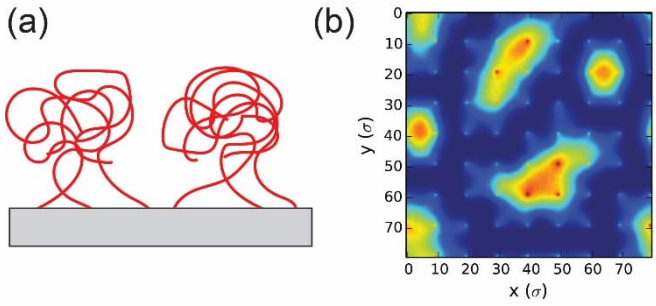

Figure 3. Collapse of polyelectrolyte brushes in the presence of multivalent counterions. (a) Formation of lateral inhomogeneities in a collapsed polyelectrolyte brushes. (b) MD simulations show that multivalent-ion induced effects drive strong phase separation of polyelectrolyte brushes. Reproduced from Ref[33].

3. SFA measurements on polyelectrolyte brushes

3.1 The SFA technique

The surface forces apparatus (SFA) has been a powerful technique for measuring interactions in polymer brush systems for decades. Early SFA direct force measurements on polyelectrolyte brushes used block copolymers containing polyelectrolyte blocks with anchor, uncharged

polymer blocks[35]. The anchor block absorbed on mica surfacs with moderate densities that typically generated low grafting density polyelectrolyte brushes. However, recent developments in surface-initiated (SI) polymerizations have greatly changed this picture. Various polyelectrolyte brush systems have been synthesized on mica surfaces through different SI polymerization methods and tested by the SFA technique (Fig. 4a).[29d, 36]

The SFA technique directly measures the force F, attractive or repulsive, between two surfaces with a crossed-cylinder geometry (locally identical to a sphere–sphere or sphere–flat geometry) as a function of the distance between the surfaces. Mica is the standard substrate for SFA measurements because it is molecularly smooth. Typically, SFA surfaces are made with freshly cleaved, uniformly thick muscovite mica sheets, back-silvered with 55 nm of silver, then glued onto half-cylindrical silica disks with a radius of curvature of $R \sim 2$ cm. The distance between the surfaces (or confined film thickness) D is measured with an optical technique based on multiple beam interference fringes (fringes of equal chromatic order, FECO) where D is determined with a resolution of ± 1Å from measurements of the wavelengths of the FECO fringes in a spectrometer. D is controlled by a series of coarse and fine micrometers and piezoelectric crystals. F is determined with an accuracy of 10 nN from the deflection of a double cantilever spring of stiffness K supporting the lower surface. It is customary to normalize the force F by R when comparing different SFA measurements. The normalized force F/R between the two cylindrical SFA surfaces is directly proportional to the energy between two flat surfaces by the Derjaguin approximation[37],

$$E(D) = F(D)/2\pi R \tag{6}$$

3.2 Normal and friction force measurements with SFA

Surface force measurements have been widely employed to explore the structure of polyelectrolyte brushes in monovalent salt solutions. Balastre *et al*. investigated the effect of monovalent counterions on the structure of physisorbed poly (*t*-butylstyrene)-*b*-poly(styrene sulfonate) brushes.[24a, b] The study confirmed the transition from the *osmotic brush* to the *salted brush* regime, and the almost-stoichiometric incorporation of counterions within the brush. Above a salt concentration of 0.02 M, the PSS brush height shrinks upon the addition of monovalent salt with an approximately −1/3 power-law relationship (Fig 4b). In addition, the study showed that the force curves never extended beyond 70% of the contour length of the PSS block, and all the curves collapsed into a master curve when rescaled with the ansatz of locally electroneutral brushes. A similar *osmotic brush* to *salted brush* transition has also been reported by Yu et al. using dense PSS brushes synthesized via SI-ATRP (Fig 4c).[29d]

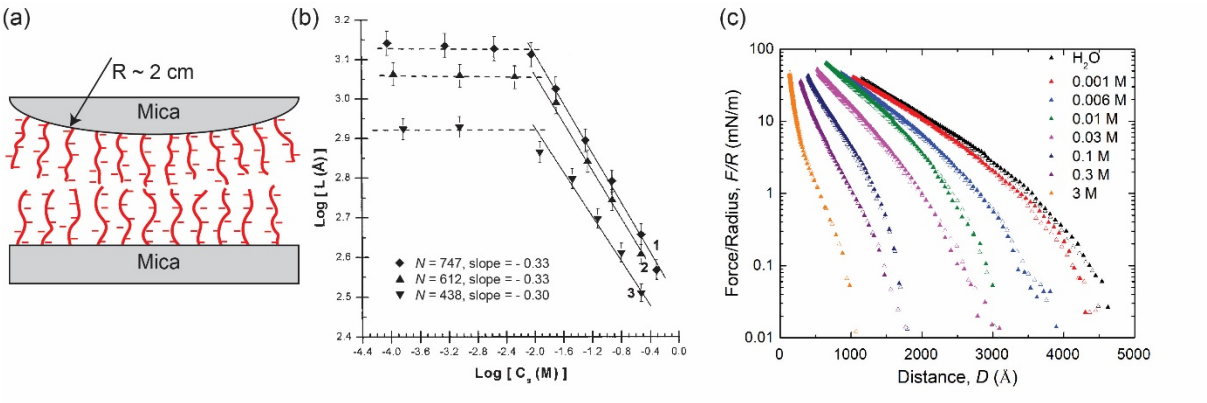

Figure 4. (a) Schematic of a surface forces apparatus (SFA) measurement on PSS brushes. (b) Salt concentration dependence of the brush height for the three PSS brushes with different chain lengths of the PSS block. Reprinted and adapted with permission from Ref.[24b]. Copyright (2002) American Chemical Society. (c) SFA force–distance curves measured during compression and separation of two identical, dense PSS brushes in pure H_2O and in $NaNO_3$ salt solutions with different concentrations. Reprinted and adapted with permission from Ref.[29d]. Copyright (2016) American Chemical Society.

Multivalent counterions can cause dramatic structural changes in polyelectrolyte brushes due to the entropy-driven ion exchange process and electrostatic crosslinks. Tirrell and co-workers conducted SFA measurements with PSS brushes in solutions containing different divalent and trivalent counterions at fixed ionic strength.[29a, b, d] Compared to monovalent counterions, divalent and trivalent counterions can cause rapid collapse of polyelectrolyte brushes in both the *osmotic brush* and *salted brush* regimes,[29a, b] as indicated by the rapid decrease of the range of repulsive forces between two PSS brushes synthesized via SI-ATRP.[29d] Additionally, attractive forces were measured when separating two physisorbed PSS brushes in the presence of trivalent $Ru(NH_3)_6^{3+}$ and La^{3+}, but the attractions induced by La^{3+} were stronger than these caused by $Ru(NH_3)_6^{3+}$, presumably due to the smaller hydration radius of La^{3+}. The attraction appears to be grafting density dependent, as no attractive force was measured between two dense PSS brushes in the presence of trivalent Y^{3+} due to the decrease of chain interpenetration.[29d]

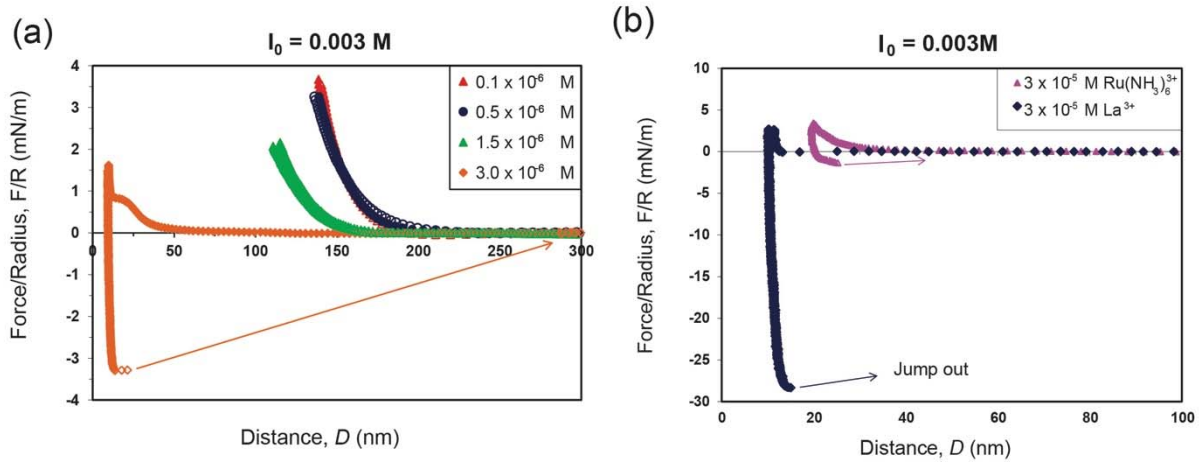

Figure 5. Surface force–distance curves of two physisorbed PSS brushes interacting in the presence of trivalent La^{3+}. (a) The range of repulsion rapidly decreases in the presence of trivalent counterions. (b) Attractive forces were measured when separating two physisorbed PSS brushes in the presence of trivalent $Ru(NH_3)_6^{3+}$ and La^{3+}. Reprinted and adapted with permission from Ref.[29b]. Copyright (2015) American Chemical Society.

The collapse of polyelectrolyte brushes is largely due to multivalent ion mediated interchain crosslinks.[33] Both divalent and trivalent counterions can cause the collapse of polyelectrolyte brushes, but divalent ions show a large ion specificity.[29d] The collapse of PSS brushes follows a trend of $Ba^{2+} > Ca^{2+} > Mg^{2+}$. Such a trend follows the order of the radii of the ions.[29d] The collapse of the PSS brushes in the presence of multivalent counterions is largely reversible, and the ions can be replaced by monovalent counterions upon increasing the monovalent ion concentration.

Polyelectrolyte brushes provide excellent wear protection and lubrication in many technical, medical, physiological, and biological applications, and this has attracted wide interest among researchers. The SFA is particularly suitable for measuring the friction and lubrication forces of polyelectrolyte brush systems due to its ability to simultaneously measure the friction forces as well as the contact area between two surfaces at controlled sliding speeds and loads.[11b, 38] Raviv et al. measured the frictional forces between sulfonated polyelectrolyte brushes with the coefficient of friction, μ, lower than 0.0006–0.001.[4b] The wear resistance and low friction are attributed to counterion osmotic pressure and the hydration layer surrounding the charged polymer segments.[39] Excellent lubrication properties were also observed using diblock copolymer with the hydrophobic block absorbed on the substrate, while the hydrated polyelectrolyte brush layer was exposed to shear forces.[38c] Klein and co-workers also designed and studied lubrication effects of polyzwitterionic brushes based on the assumption that the good lubrication properties of polyelectrolyte brushes are due to strong hydration of the polyelectrolytes.[11b, 36, 40]

4. AFM measurements on polyelectrolyte brushes

4.1 The AFM technique

Atomic force microscopy[41] (AFM) is based on measurements of the forces between a sample and a small tip (radius of curvature typically 5–50 nm) or sphere ("colloidal probe", with a radius of a few micrometers) attached to the end of a cantilever commonly made of silicon or silicon nitride. The deflection of the cantilever in response to attraction or repulsion between the sample and tip or probe is measured (typically by reflecting a low-power laser beam off the end of the cantilever) and converted into normal force as a function of sample position in the normal direction. Depending on the setup, either the sample or the cantilever can also be moved laterally so that normal forces can be measured at different locations of the sample ("force volume" measurements). Images of different surface features or properties can be obtained by moving the sample or cantilever laterally back-and-forth (scanning) over a chosen region of the surface and using a feedback system to either keep the deflection (normal force or load) of the cantilever constant (in contact mode) or controlling its oscillation amplitude or frequency (in tapping mode or non-contact mode). The topography (height) and, in the case of tapping

mode, viscoelastic response of the sample surface can then be obtained from the measured signals. The torsion of the cantilever can also be measured during scanning in contact mode to obtain friction forces at a chosen normal force (load).

The length scales and contact areas accessed with a sharp tip and a colloidal probe are very different. In both cases, they are smaller than those accessed with the SFA. Another important difference between the AFM and SFA is that the distance or film thickness in the SFA is measured with respect to the bare substrate, which is commonly not the case with AFM. AFM force measurements are also more complicated to calibrate than the SFA. Because of the small area over which the interaction occurs, AFM with sharp tips is suitable for measurements of small (nN), short-range forces and for imaging with high resolution. The colloidal probe technique is suitable for measurements of longer-range interactions like electrostatic double-layer forces. The tip or colloidal probe can be bare (covered with native oxide layers or metal/metal oxides) or functionalized with, for example, self-assembled monolayers or polyelectrolyte brush layers. The sample can be any material of interest – the survey below will focus on fairly flat substrates covered with polyelectrolyte brush layers. In particular when working with functionalized sharp tips, it is worth noting that the packing density and response of a self-assembled monolayer or brush layer on a strongly curved surface can differ from that on a planar one.

4.2 Normal and friction force measurements with AFM

The utility of AFM force measurements has been shown for various polyelectrolyte brush systems (including single-component strong[42] and weak[42c, 43] polyelectrolytes, mixed weak polyelectrolytes[44] and zwitterionic brushes[45]). Sharp tips may penetrate in between extended chains or strongly deform soft regions and can be used to obtain information on the innermost structure of the layer and possible aggregation there,[42c, 44] whereas colloidal probes, because of their larger contact area, typically probe the outermost regions of the brush and its response to compression at low to moderate pressures (closer to the brush height and applied pressure region investigated in the SFA). As with the SFA, a wealth of information on different types of interactions between the extended chains and an apposing surface as well as chain interactions within the brush on compression can be inferred from the force measurements.

It has been shown that single-molecule spectroscopy with a sharp tip can be used to obtain values of contour length and persistence length of molecules formed from grafting-from procedures.[43a] Normal force measurements with a sharp tip or colloidal probe can be used (in a similar manner to SFA force measurements) to distinguish electrostatic double-layer forces from steric ones and thus used to investigate the swelling of brushes in different solvents and salt concentrations,[42a, b, 43d, e, 44] detect collapse and recovery of the layer at different normal forces and solution conditions,[42a, d, 43d] including the effects of monovalent and divalent counterions with different hydration and ability for ion-pairing,[42d] and the development of adhesion between strongly compressed layers due to interactions between hydrophobic backbones in cases of highly screened or ion-paired systems.[43d, e, 44]

Friction measurements with sharp tips have shown that the response depends on the extension and rigidity of the brush layer, typically giving linear friction and lower friction coefficients in non-adhesive systems (i.e., where the brushes are strongly extended) and non-linear friction when the brushes are collapsed and the probe adheres to the surface,[43e, 45] similarly to in non-charged brush systems that respond to solvent quality.[46] The friction coefficients are typically

not as low as the ones measured with the SFA, which is ascribed to penetration of the sharp tip into the extended layers.

4.3 Structures observed by AFM imaging

A very important aspect of AFM is its imaging capability. For studies of polyelectrolyte brushes, it is particularly useful to image the brushes when immersed and equilibrated in liquids of different pH or electrolyte concentrations to obtain information on their collapsed structures (aggregated versus homogeneous film structures).[42c, d, 44] By patterning the substrate with brush regions separated by bare substrate,[42a, c] or by scratching the surface before or during the experiment to remove the polyelectrolyte brush in certain areas,[44] mages can give information on the total height of the brush layer (dry or extended to different height in different solvents) and its compressibility and recovery.

Figure 6 shows AFM tapping mode height (topography) and phase images of PSS brushes in different salt solutions. In monovalent salt (Na^+), the polyelectrolyte chains are extended and the top of the brush is fairly uniform in height (small variations are due to the polydispersity and thermal fluctuations in chain length) and very uniform in phase, suggesting a homogenous layer with uniform viscoelastic properties. In contrast, a low concentration of Y^{3+} (cf. Figure 5) causes a collapse of the brush to a heterogeneous film with apparent aggregation ascribed to the bridging of different chains by the multivalent ions.[33]

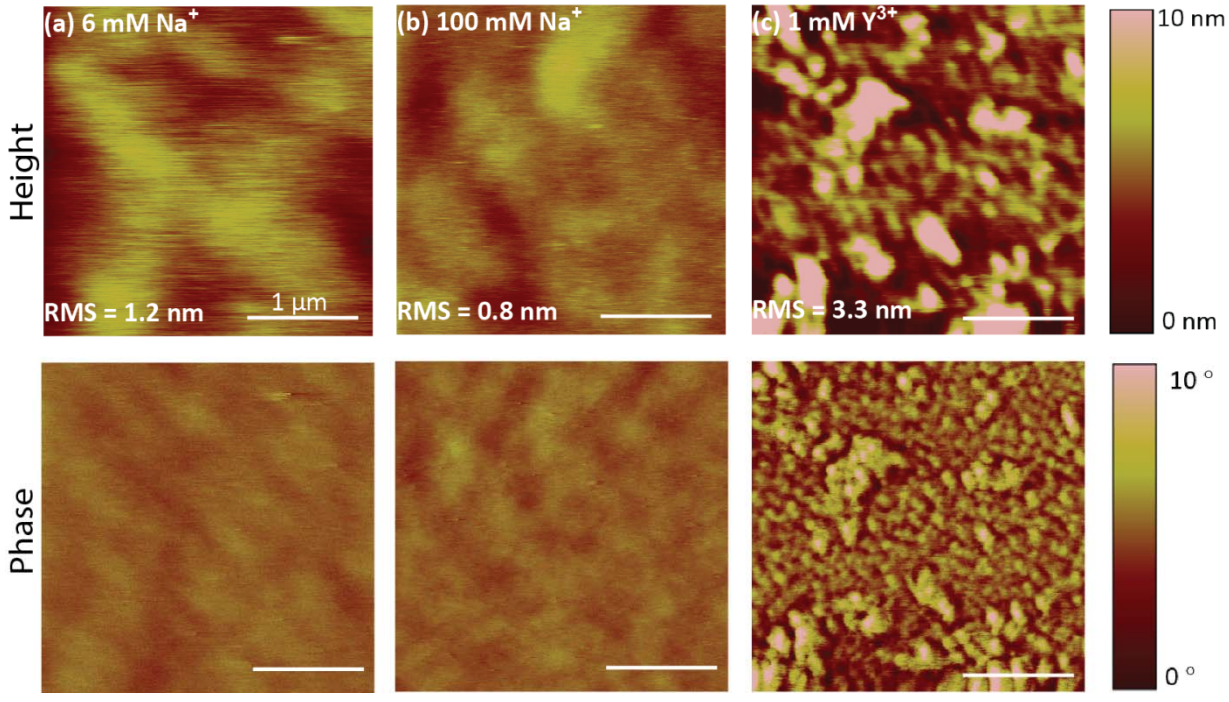

Figure 6. Tapping mode AFM images of PSS brushes in aqueous solutions containing different concentrations of Na^+ or Y^{3+}. Top row: Height (topography), bottom row: Phase. Scan size 3 µm × 3 µm.

5. Nonfouling Polyelectrolyte Brushes

Poly(2-hydroxyethyl methacrylate) (PHEMA) and poly(poly(ethylene glycol methacrylate)) (PPEGMA) brushes are very effective surface coatings to prevent the non-specific adsorption

of proteins, cells and bacteria, amongst others.[47] One drawback of PHEMA and PPEGMA type polymer brush coatings is that the side chains of these surface grafted polymers are susceptible to decomposition and auto-oxidation reactions, which can result in the formation of reactive aldehyde moieties and compromise the nonfouling behavior of the polymer films.[48] S. Jiang and coworkers have been exploring zwitterionic polysulfobetaine and polycarboxybetaine brush films as alternative platforms for the fabrication of non-fouling polymer brush surfaces.[48a, 49] Table 1 provides an overview of non-fouling polyelectrolyte brushes that have been prepared via surface-initiated atom transfer radical polymerization (SI-ATRP). A comparative study that used zwitterionic poly(carboxybetaine methacrylate) (PCBMA) and poly(3-[dimethyl(2`-methacryloyloxyethyl)ammonio] butanesulfonate) (PMABS) brushes with thicknesses of ~ 10–15 nm and a PPEGMA brush with a thickness of 20–25 nm revealed similar levels of non-specific protein adsorption from human plasma and human serum onto PMABS and PPEGMA. In this study, the PCBMA film even outperformed the nonfouling behavior of the PPEGMA and PMABS polymer brushes.[48a]

To emulate the outstanding non-fouling properties of zwitterionic polymer brushes, the copolymerization of mixtures of positively and negatively charged monomers has been investigated. Copolymerization of PSPMA with (2-(acryloyloxy) ethyl) trimethyl ammonium chloride (METAC), for example, in a 2:1, 1:1 or 1:2 monomer feed ratio resulted in polymer brush films that showed improved resistance to the non-specific absorption of fibrinogen (FBG), bovine serum albumin (BSA) and lysozyme (LYZ) as compared to a PSPMA homopolymer brush film (Figure 7A).[50] Tah and Bernards studied the influence of film thickness on the non-specific adsorption of LYZ on copolymer brush films that were composed of equimolar amounts of METAC and carboxyethylacrylate CAA (Figure 7B).[48b] From these experiments, the authors concluded that the ideal film thickness for a P(METAC-co-CAA) to prevent non-specific adsorption of LYZ is in the range of 18 to 30 nm.

Table 1: Overview of nonfouling polyelectrolyte brushes prepared via SI-ATRP.

Polymer brush	**Substrate**	**Film thickness [nm]**	**Grafting density [chains/ nm^2]**	**Nonfouling properties**	**Ref.**
PMAES (*n* = 2)/PMAPS (*n* = 3)/PMABS (*n* = 4) 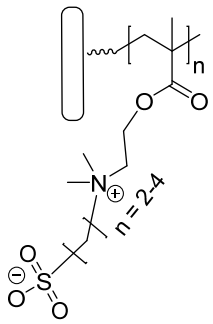	Si wafer	173 (PMAES) 105 (PMAPS) 115 (PMABS)	0.19 (PMAES) 0.26 (PMAPS) 0.52 (PMABS)	*Barnacle Cypris Larva* (% settled): Si wafer 65 %; PMAES 2 %; PMAPS 7 %; PMABS 0 %. *Mussel Larva* (% settled): Si wafer 75 %; PMAES 10 %; PMAPS 7 %; PMABS 0 %. *Marine bacteria* (colonies per field of view): Si wafer 230; PMAES 30; PMAPS 50; PMABS 60.	[51]
PMABS 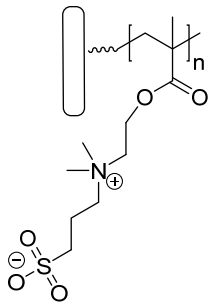	Stainless steel	132 ± 16	N. A.	*Amphora coffeaeformis* (cells/cm^2): Pristine SS 1350; PMABS settled 3900. *Barnacle Cyprids Larvae*: Pristine SS 85%; PMABS Settled 1%, Dead 10%. *Pseudomonas sp* : No Nrs. Available.	[52]
	SPR chip gold	10–15	N. A.	*Human Serum* (pg/mm^2): 10 % Serum ~ 50; 100 % Serum ~ 400. *Human Plasma* (pg/mm^2): 10 % plasma 10; 100 % plasma 100.	[48a]

PSBMAm 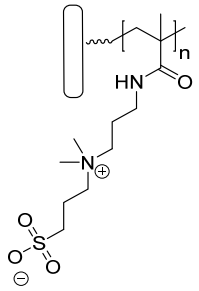	PDMS	10 (dry) 50–60 (0.7 M NaCl)	N. A.	*Amphora coffeaeformis* (# settled/mm^2). PDMS-FDTS: Smooth 110; Patterned 95. SBMAm: Smooth 120; Patterned 75. *Amphibalanus Amphitrite* (Fraction settled/ mm^2): PDMS-FDTS: Smooth 0.42; Patterned 0.48. SBMAm: Smooth 0.50; Patterned 0.21.	[53]
PMETAC 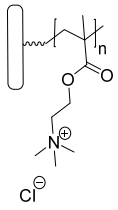	Si wafer	110	0.33	*Barnacle Cypris Larva :* Si wafer 65 % ; PMETAC 10 days 0%. *Mussel Larva :* Si wafer 75 % ; PMETAC 72 %. *Marine bacteria* (colonies per field of view): Si wafer 230; PMETAC 250.	[51]
	Stainless steel	111± 13	N. A.	*Amphora coffeaeformis* (cells/cm^2): Pristine SS 1350; PMETAC settled 3900. *Barnacle Cyprids Larvae* : Pristine SS 85 %; PMETAC Settled 8 %, Dead 10 %. *Pseudomonas sp* : No Nrs. Available.	[52]
P(METAC-*co*-SPMA)	SPR gold chip	Ratio (METAC): (SPMA)	N. A.	*FBG* (ng/cm^2): 1/0 : 1050; 2/1 : 15; 1/1 : 2;	[50]

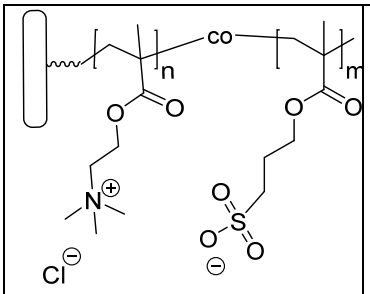		1/0: 15.6 ± 3; 2/1: 24.3 ± 7; 1/1: 35.4 ± 12; 1/2: 39.6 ± 7; 0/1: 35.1 ± 14		1/2 : 1; 0/1 : 40. *LYZ* (ng/cm^2): 1/0 : 2; 2/1 : 1; 1/:12; 1/2 : 250; 0/1 : 1400. *BSA* (ng/cm^2): 1/0 : 450; 2/1 : 2; 1/1 : 1; 1/2 : 8; 0/1 : 6.	
P(METAC-*co*-CAA) 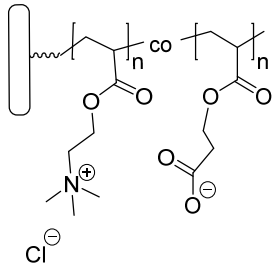	Si wafer	50	N. A.	*FBG* (ng/cm^2): 17 *LYZ* (ng/cm^2): 8 *FBG conjugation* (ng/cm^2): 15	[48b]
PCBMA 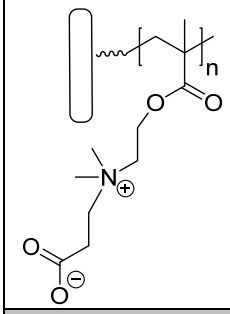	SPR chip gold layer	10–15	N.A.	*Human Serum* (pg/mm^2): 10 % Serum ~ 0; 100 % Serum ~ 50. *Human Plasma* (pg/mm^2): 10 % Plasma 5; 100 % Plasma 100.	[48a]
PMPC 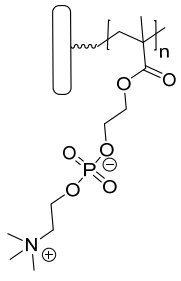	Si wafer	85	0.20	*Barnacle Cypris Larva:* Si wafer 65 % ; PMPC 10 days 1%. *Mussel Larva :* Si wafer 75 % ; PMPC 0%. *Marine bacteria* (colonies per field of view): Si wafer 230; PMPC 70.	[51]
	Stainless steel	53 ± 1.0	N.A.	*Amphora coffeaeformis* (cells/cm^2) *:* Pristine SS 1350;	[52]

				PMPC 3800. *Barnacle Cyprids Larvae*: Pristine SS 85 %; PMPC Settled 2 %, Dead 8 %. *Pseudomonas sp. :* No Nrs. Available.	
PVBIPS 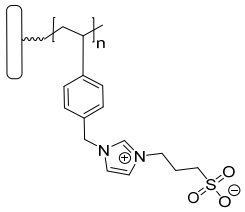	SPR gold chip	28 (dry)	N.A.	*Blood Serum* (ng/cm^2): Serum-PBS 105; Serum-NaCl 2. *Blood Plasma* (ng/cm^2): Plasma-PBS 130; Plasma-NaCl 30. *Bacterial Pseudomonas aerinosa and staphylococcus epidermidis:* No Nrs. available.	[54]
	SPR gold	6-125	N.A.	*Blood serum and Blood plasma* (ng/cm^2): 140-145; 18-0.23 after 1.0 m NaCl .	[17]

PMAES = poly(3-[dimethyl(2`-methacryloyloxyethyl)ammonio] ethanesulfonate, PMAPS = poly(3-[dimethyl(2`-methacryloyloxyethyl)ammonio] propanesulfonate), PMABS = poly(3-[dimethyl(2`-methacryloyloxyethyl) -ammonio] butanesulfonate), PMPC = poly(2-methacryloyloxyethyl phosphorylcholine), PMETAC = poly([2-(methacryloyloxy)ethyl]trimethylammonium chloride), P(VBIPS) = poly(3-(1-(4-vinylbenzyl)-1H-imidazol-3-ium-3-yl)propane-1-sulfonate), PCBMA = poly(carboxybetaine methacrylate), PSBMAm = poly([3-methacryloylamino) -propoyl] dimethyl(3-sulfopropyl) ammonium hydroxide inner salt, PSPMA = poly(3-sulfopropyl methacrylate potassium salt), PCAA = poly(carboxyethyl acrylate).

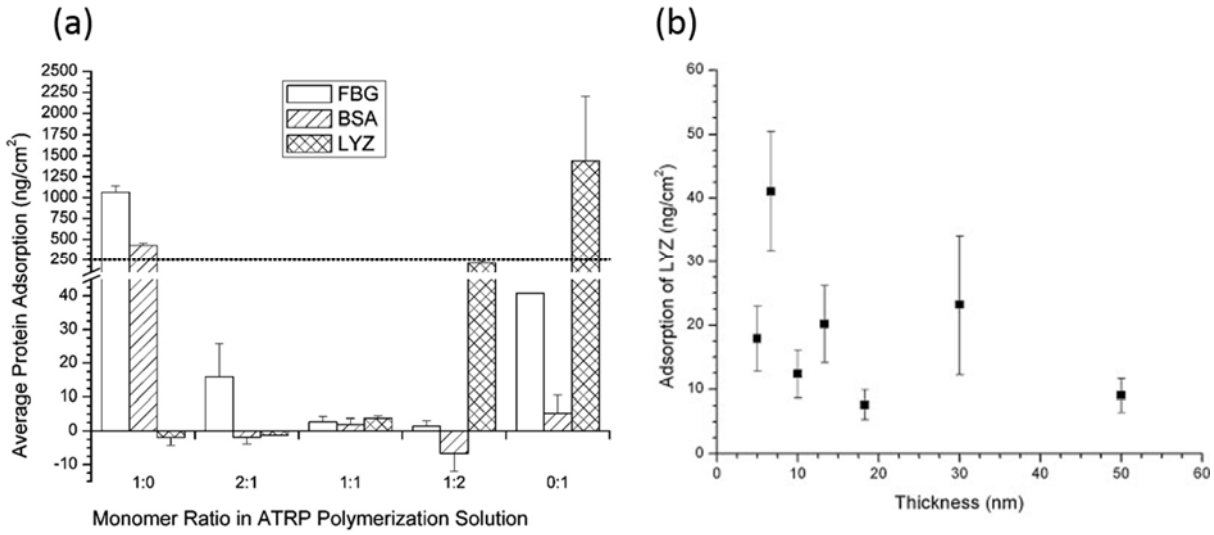

Figure 7: (a) Adsorption of FBG (clear bars), BSA (diagonal lines), and LYZ (cross hatch) to P(METAC-co-PSPMA) copolymer brush-coated surfaces of different compositions as measured by surface plasmon resonance (SPR). Each bar represents the average (SE for the adsorption of each protein to each polymer ratio, measured on three separate samples (n = 3). The dotted line represents a monolayer of adsorbed protein, ~250 ng/cm^2, based on the amount of FBG that adsorbs to a methyl-terminated SAM (Reprinted and adapted with permission from Ref.[50], Copyright (2008) American Chemical Society). (b) Average ± standard error of the mean of nonspecific adsorption of LYZ to P(METAC-*co*-CAA) copolymer brushes of different film thicknesses as measured by SPR. Six independent experiments were run at each copolymer brush thickness (n = 6). Reprinted and adapted with permission from Ref.[48b], Copyright (2012) with permission from Elsevier.

More recently, an interesting and less explored zwitterionic monomer, 3-(1-(4-vinylbenzyl)-1H-imidazol-3-ium-3-yl)propane-1-sulfonate (VBIPS) was investigated by Zheng et al. to produce polymer brush films via SI-ATRP (Figure 8).[17, 54] The hydrophobic imidazole moiety not only avoids hydrolysis but also confers unique, ionic strength dependent swelling properties to the PVBIPS brush films. At high ionic strengths, surface grafted PVBIPS chains adopt a more extended chain conformation and are more resistant to nonspecific protein adsorption.[54] The ionic strength dependent fouling properties make these polymer brush films very interesting for the reversible surface capture and release of proteins.[17]

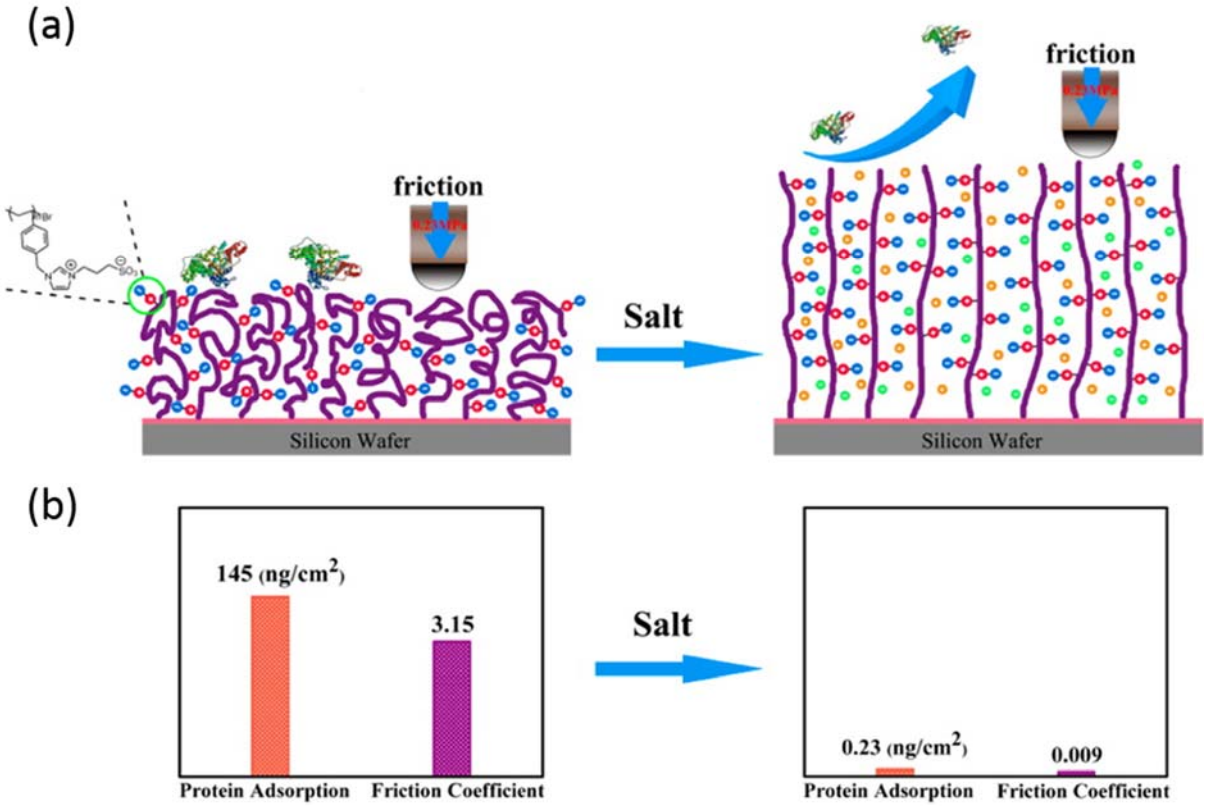

Figure 8 (a) Schematic illustration of the structure of a PVBIPS brush and the change in conformational properties upon exposure to high ionic strength solutions; (b) Changes in protein adsorption and friction coefficient of PVBIPS brush films upon exposure to high ionic strengths. Reprinted and adapted with permission from Ref.[17], Copyright (2015) American Chemical Society.

Zwitterionic polymer brushes have attracted significant interest to prevent marine biofouling. Higaki et al. performed an extensive study in which the settlement of barnacle cypris larva, mussel larva and marine bacteria on zwitterionic PMPC, PMAES, PMAPS and PMABS brushes was compared with that on hydrophobic brush modified surfaces, a cationic polymer brush (PMETAC) functionalized substrate as well as with unmodified silicon wafers (Figure 9).[51] In these experiments, the zwitterionic polymer brush modified surfaces showed an excellent resistance towards the settlement of barnacle cypris larva and mussel larva as compared to the hydrophobic brush coated silicon wafers.

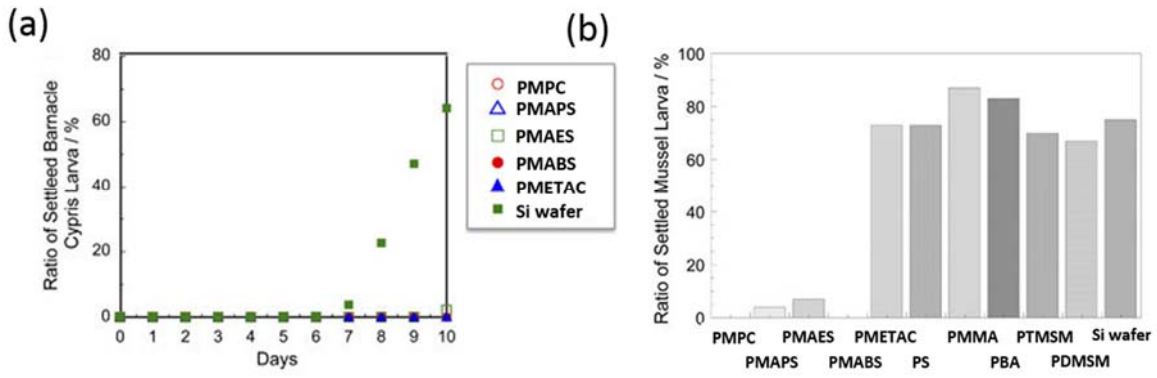

Figure 9: (a) Evolution of the ratio of 'settled' barnacle cypris larva on several zwitterionic and cationic polyelectrolyte brushes and an unmodified silicon wafer; (b) Percentage of 'settled' mussel larva counted after a settlement test period of 6 days on various polymer brush coated surfaces and an unmodified silicon wafer. Reprinted and adapted with permission from Ref.[51], Copyright (2012) with permission from Wiley. PS = poly(styrene), PBA = poly(butyl acrylate), PTMSM = poly(3-[tris(trimethylsiloxy)silyl]propylmethacrylate), PDMSM = poly(3-(poly(dimethylsiloxy) propylmethacrylate).

Brzozowska et al. demonstrated that the marine antifouling properties of zwitterionic polymer brushes not only depend on the surface chemistry, but can also be tuned by engineering the surface topography. To this end, the ability of both planar as well as microstructured polydimethylsiloxane (PDMS) substrates modified with a PSBMAm brush coating to prevent barnacle settlement and algae adhesion was studied.[53] The performance of the polymer brush coated substrates was compared with that of 1*H*,1*H*,2*H*,2*H*-perfluorododecyltrichlorosilane (FDTS) functionalized PDMS substrates, PDMS substrates covered with a layer-by-layer (LbL)-deposited polyelectrolyte film generated from poly(isobutylene-*alt*-maleic anhydride) and polyethyleneimine as well as unmodified glass (Figure 10). These experiments demonstrated that settlement of *Amphora coffeaeformis* and *Amphibalanus Amphitrite* on PSBMAm brush coated micropatterned PDMS surfaces was reduced as compared to smooth PDMS films that were modified with the same polymer brush.

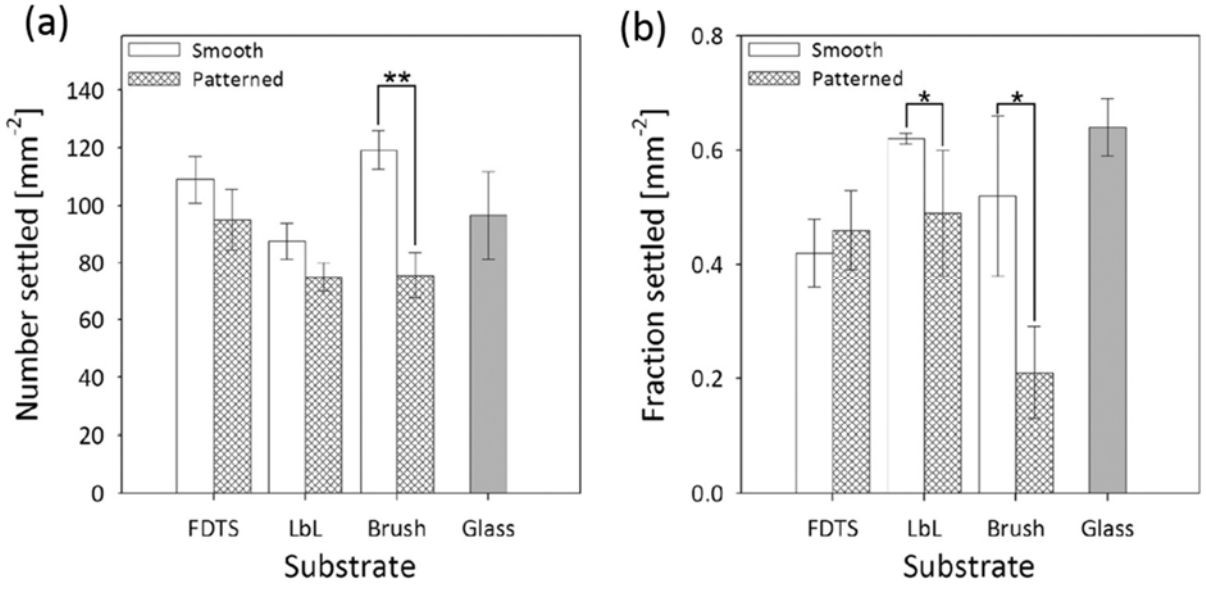

Figure 10: Settlement of *Amphora coffeaeformis* (a) and *Amphibalanus amphitrite* (b) on smooth and patterned PDMS samples modified with FDTS, LbL films, and sulfobetaine brushes. The data are shown as the total number of settled organisms (a) and the fraction of settled organisms (b) per square millimeter. The notation for the statistical significance was adapted as follows: * = $0.05 \leq p < 0.10$, ** = $0.01 \leq p < 0.05$, *** = $p < 0.01$. Reprinted and adapted with permission from Ref.[53], Copyright (2014) American Chemical Society.

6. Polyelectrolyte brush-based boundary lubricants

Friction occurs when two surfaces that are in contact slide against each other in opposite direction. This includes not only gearwheels in large industrial equipment and in watches but also movements of the joints of hips and knees. Reducing friction thus is not only of great technological relevance, but also critical to ensure smooth and painless movement of joints in the human body. Surface-grafted polyelectrolyte brushes are a very attractive class of aqueous boundary lubricants.[55] Much of the current interest and activities in this area are based on pioneering work by Klein and coworkers. In a paper, which was published in 2009, these researchers reported that zwitterionic PMPC brushes were able to provide extremely efficient lubrication in aqueous media.[11b] For these brushes, friction coefficients $\mu \approx 0.001$ were measured at pressures up to 7.5 MPa, which are comparable to those in the synovial joints of humans. The extraordinary performance of these polymer brushes was attributed to the strongly hydrated MPC monomers, which are highly and tenaciously hydrated, yet allow rapid exchange of bound water molecules with other hydration or free water molecules. Table 2 provides an overview of polyelectrolyte brushes prepared by surface-initiated polymerization, which have been studied as boundary lubricants.

Table 2: Overview of polyelectrolyte brushes prepared by surface-initiated polymerization, which have been studied as boundary lubricants.

Polymer brush	Substrate	Film thickness [nm]	Grafting Density [chains/ nm^2]	Lubrication properties	Ref.
PSPMA 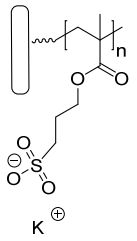	Cr coated steel	80 (dry) 210 (water)	0.2–0.5	Slider on disk aperture. Tribo pair: glass/polyelectrolyte coated slider: load = 0.13 MPa: μ = 0.006	[56]
	Gold coated resonator	26 ± 4	N. A.	Sliding velocity of a PDMS cylinder (d = 6 mm) on polyelectrolyte coated surface with an angle of inclination of 10°: v_s = 6.4 ± 0.2 cm/s (pH 2); v_s = 7.6 ± 0.3 cm/s (pH 7); v_s = 8.3 ± 0.3 cm/s (pH 12).	[57]
	Si wafer	N. A.	N. A.	Ball-on-plate tribometer. Tribo pair: polyelectrolyte coated glass ball and polyelectrolyte coated Si wafer: v_s = 1.5 x 10^{-3} m/s, load = 0.49 N (50 g), pressure = 139 MPa: μ = 0.018 (water), 0.4 (dry N_2) and 0.1 (humid air).	[58]
	Si wafer	50	N. A.	Ball on plate type tribometer. Tribo pair: polyelectrolyte coated glass ball and polyelectrolyte coated Si wafer: v_s = 1.5 x 10^{-3} m/s, load = 0.49 N, pressure = 140 MPa: μ = 0.08 (water);	[41b]

				0.42 (dry N_2); 0.1 (humid air). Tribo pair: glass ball /polyelectrolyte covered wafer: μ = 0.018 (water); 0.45 (dry N_2).	
	Gold coated Si wafer	45	N. A.	Sliding silicone hemi-sphere on a polyelectrolyte covered Si wafer: v_s = 2 x 10^{-3} m/s, load = 0.5 N, pressure = 0.23 MPa: μ = 0.005 (PSPMA-K^+); 0.013 (PSPMA-TBAB); 0.24 (PSPMA CTAB); 0.008 (PSPMA-Cu^{2+}); 0.011 (PSPMA-Fe^{3+}).	[59]
Poly(SPMA-*co*-METAC) 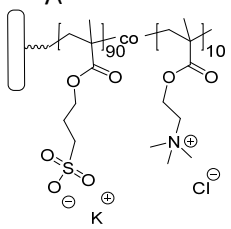	Si wafer	N. A.	N. A.	Ball on plate type tribometer. Tribo pair: silicone elastomer ball and poly-electrolyte coated Si wafer: v_s = 1.5 x 10^{-3} m/s, load = 0.49 N and pressure = 139 MPa: μ = 0.015.	[58]
PMABS 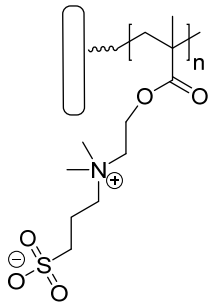	Gold coated Si wafer	15	N. A.	Silicone hemisphere and polyelectrolyte coated Si-wafer: v_s = 2 x 10^{-3} m/s, load = 0.5 N, pressure = 0.23 MPa: μ = 0.005 (PMABS-TBAB); 0.006 (PMABS-DTAB); 0.007 (PMABS-CTAB); 0.008 (PMABS-$TFSI^-$); 0.010 (PMABS-PF_6^-); 0.09 (PMABS-ClO_4^-); 0.006 PMABS (water).	[59]
PMPC	Mica	12.2 and 28.2	4.2 ± 1 Bromine per nm^2	Surface force balance (load of 2−7.5 MPa): μ = 0.00043 (water); 0.001 ± 0.0004 (0.01 M $NaNO_3$);	[60]

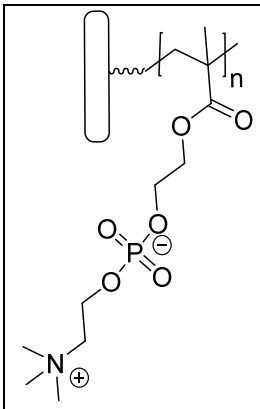				0.0026 + 0.0005 - 0.001 (0.1 M $NaNO_3$).	
	Si wafer	N. A.	N. A.	Ball on plate type tribometer. Tribo pair: glass ball and polyelectrolyte coated Si-wafer: v_s = 1.5 x 10^{-3} m/s, load = 0.49 N, pressure =139 MPa: μ = 0.08.	[58]
	Si wafer	50	0.23	Ball on plate tribometer. Tribo-pair: polyelectrolyte coated glass ball and polyelectrolyte coated Si wafer: v_s = 1.5 x 10^{-3} m/s, load = 0.49 N, pressure = 140 MPa: μ = 0.16 (dry N_2); 0.04 (water); 0.03 (humid air). Tribo pair: glass ball on polyelectrolyte coated Si wafer: μ = 0.215 (dry N_2); 0.125 (water).	[41b]
Poly(MPC-*co*-DMAEMA) 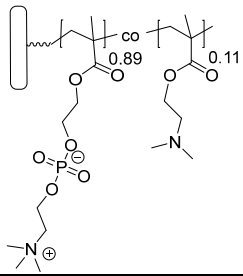	Si wafer	85 (dry)	N. A.	Ball on plate tribometer. Tribo pair: glass ball and polyelectrolyte coated Si wafer: v_s = 1.5 x 10^{-3} m/s, load of 0.49 N, pressure = 139 MPa: μ = 0.115.	[58]
Crosslinked PMPC	Si wafer	Post-polymerization modification of 85 nm thick poly(MPC-co-DMAEMA) brush	N. A.	Ball on plate tribometer. Tribo pair: glass ball and polyelectrolyte coated Si wafer: v_s = 1.5 x 10^{-3} m/s, load =0.49 N, pressure = 139 MPa: μ = 0.12.	[58]

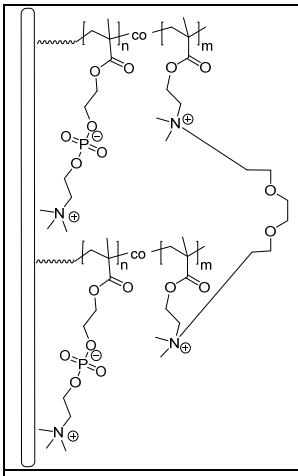					
Poly(MPC-*co*-METAI) 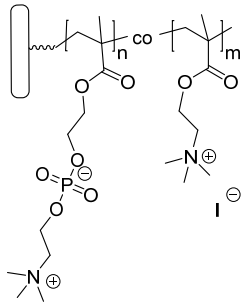	Si wafer	Post-polymerization modification of 85 nm thick poly(MPC-co-DMAEMA) brush	N. A.	Ball on plate tribometer. Tribo pair: glass ball and polyelectrolyte coated Si wafer: v_s = 1.5 x 10^{-3} m/s, load = 0.49 N, pressure = 139 MPa: μ = 0.14.	[58]
PMETAC 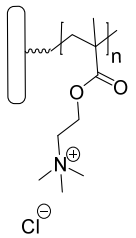	Glass disk or silicon wafer	170 (dry)	N. A.	Glass ball on a polymer brush coated substrate: v_s = 10^{-5}-10^{-1} m/s, load = 0.49 N, pressure= 139 MPa. μ = 0.01–0.02.	[61]
	Gold coated resonator	26 ± 4	N. A.	Sliding velocity of a PDMS cylinder (d = 6 mm) on polyelectrolyte coated surfaces with an angle of inclination of 10°. v_s = 14.7 ± 0.5 cm/s (pH 2); v_s = 11.3 ± 0.6 cm/s (pH 7); v_s = 0.04 ± 0.01 cm/s (pH 12)	[57]
	Si wafer	N. A.	N. A.	Ball on plate tribometer. Tribo pair: glass ball and polyelectrolyte coated Si wafer: v_s = 1.5 x 10^{-3} m/s, load = 0.49 N:	[58]

				μ = 0.22 (dry N_2); 0.08 (water); 0.115 (humid air).	
	Si wafer	50	0.20	Polyelectrolyte covered glass ball sliding on a polyelectrolyte covered Si wafer: v_s = 1.5 x 10^{-3} m/s, load = 0.49 N: μ = 0.22 (dry N_2); 0.085 (water); 1.10 (humid air). Tribo pair: glass ball and polyelectrolyte covered wafer: μ = 0.2 (dry N_2); 0.13 (water).	[41b]
	Gold coated Si wafer	PMETAC-Cl^-: 12 (dry); PMETAC-Cl^-: 41 (water); PMETAC-$TFSI^-$: 15 (dry); PMETAC-$TFSI^-$: 18 (water).	N. A.	Sliding PDMS hemisphere on a polyelectrolyte coated Si wafer: v_s = 2 x 10^{-3} m/s, load of 0.5 N (pressure ≈ 0.23 MPa): μ = 0.006 (PMETAC-Cl^-); 0.016 (PMETAC-ClO_4^-); 0.092 (PMETAC-PF_6^-); 0.828 (PMETAC-$TFSI^-$).	[59]
PMAA 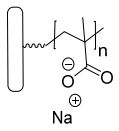	Gold coated Si wafer	PMAA 35	N. A.	Pin (PDMS hemisphere)-on-disk: v_s = 2 x 10^{-3} m/s, load = 0.5 N (0.23 MPa); μ = 0.006 (PMMA-Na^+); 0.008 PMMA-NH_4^+); 0.013 (PMMA-TBAB); 0.014 (PMAA-TEAB) 1.05 (PMMA-Cu^{2+}); 1.32 (PMMA-Fe^{3+}).	[59]
PBIM-PF_6	Multi-walled carbon	N. A.	N. A.	Brush modified MWCNTs as additives in base lubricant 1-	[62]

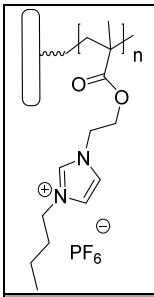	nano-tubes			methyl-3-butyl-imida-zolium hexafluoro-phosphate (LP104), using an Optimol SRV oscillating friction and wear tester a ball-on-disc contact configuration.	
PVBIPS 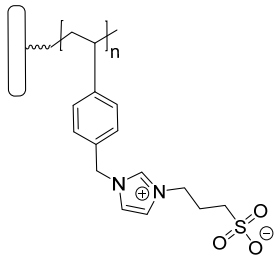	Si wafer	6 - 125	N. A.	Pin on disk tribometer with a PDMS hemisphere: v_s = 2 x 10^{-3} m/s, load = 0.5 N (0.23 MPa) : $\mu \sim 10^{-3}$. Depending on salt concentration and counterion, μ could be tuned from $\sim 10^{0}$ to $\sim 10^{-2}$ and $\sim 10^{-3}$.	[17]

PMABS = poly(3-[dimethyl(2`-methacryloyloxyethyl)ammonio] butanesulfonate), PMPC = poly(2-methacryloyl-oxyethyl phosphorylcholine), PMETAC = poly([2-(methacryloyloxy)ethyl]trimethylammonium chloride), P(VBIPS) = poly(3-(1-(4-vinylbenzyl)-1H-imidazol-3-ium-3-yl)propane-1-sulfonate), PSPMA = poly(3-sulfopropyl methacrylate potassium salt), PMAA = poly(methacrylic acid), PDMAEMA = poly(2-dimethylaminoethyl methacrylate), PMTAI = poly(2- (methacryloyloxy)ethyltrimethyl ammonium iodide), PBIM-PF_6 = poly(2-(1-butylimidazolium-3-yl) ethyl methacrylatehexafluorophosphate).

The lubrication properties of polyelectrolyte brushes very strongly depend on the nature of the counterion.[59] By varying the counterion, the friction coefficient of polyelectrolyte brushes can be tuned from ~ 10^{-3} (superior lubrication) to > 1 (ultrahigh friction) (Figure 11).

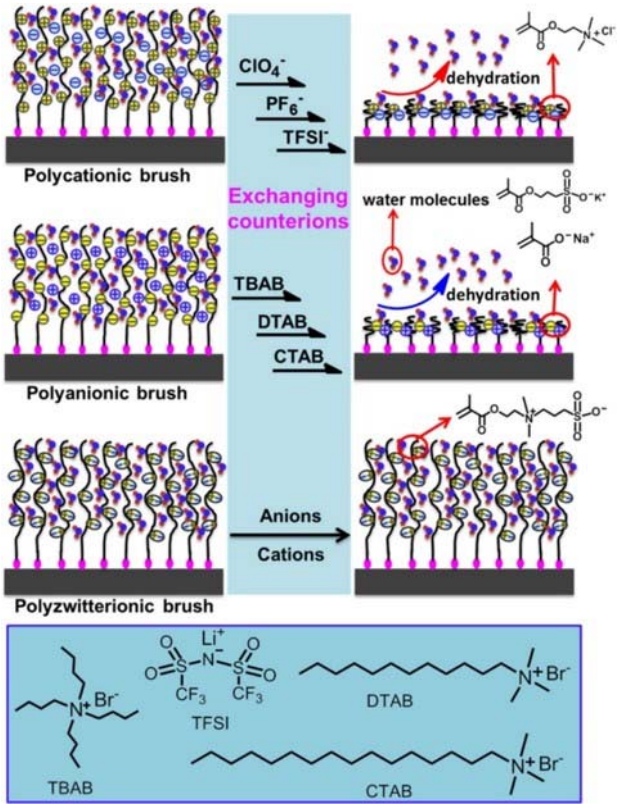

Figure 11: Schematic illustration of the conformational changes that surface-grafted polyelectrolytes undergo upon exchange of counterions. The bottom panel shows the chemical structures of the different counterions. Reprinted and adapted with permission from Ref.[59], Copyright (2013) American Chemical Society.

Wei et al. investigated the friction properties of PMETAC brushes and three homologues in which the Cl^- counterion was exchanged for ClO_4^-, PF_6^- and $TFSI^-$. Exchange of the Cl^- counterion was found to result in an increase in the friction coefficient from ~ 0.006 for the original PMETAC brush to 0.016, 0.092, and 0.828, respectively, in the ClO_4^-, PF_6^- and $TFSI^-$ homologues (Figure 12a).[59] Counterion exchange also significantly changed the wetting properties of the polymer brush surfaces, which was evidenced by an increase in the water contact angle from ~ 10° (Cl^-) to 43° (ClO_4^-), 56° (PF_6^-), and 75° ($TFSI^-$). These observations were attributed to a progressive collapse and dehydration in aqueous media, and a concomitant reduction in lubrication and wetting properties of the polymer brushes, upon exchanging the mobile Cl^- by larger, more hydrophobic anions. This was confirmed by swelling experiments on PMETAC samples and polymer brushes in which the Cl^- counterion was exchanged for $TFSI^-$. Comparison of the dry and swollen film thickness in water of a PMETAC brush

revealed a swelling ratio of ~ 3.4. Upon exchanging the Cl^- counterion with $TFSI^-$, however, the swelling ratio decreased to only ~ 1.2 (Figure 12b).

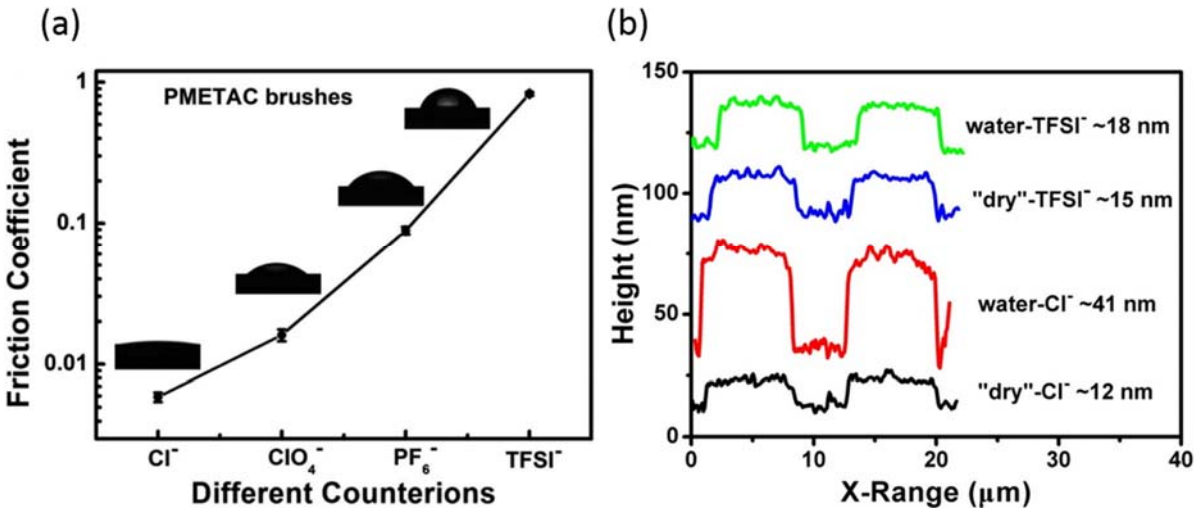

Figure 12: (a) Friction coefficient as a function of time for a PMETAC brush in water and following subsequent, in situ injection of 5 mM solutions of ClO_4^-, PF_6^-, and $TFSI^-$; (b) AFM cross-sectional profile of a PMETAC brush and a homologue containing $TFSI^-$ counterions in the "dry" state (ambient conditions, humidity: 15 %) and in water. Reprinted and adapted with permission from Ref.[59], Copyright (2013) American Chemical Society.

Wei et al. also studied the influence of counterion valence on the lubrication properties of polyanionic PSPMA and PMAA brushes (Figure 13).[59] For the PSPMA brush, the friction coefficient only slightly increased from 0.005 to 0.008 and 0.011, respectively, when K^+ was replaced with Cu^{2+} and Fe^{3+}. For the PMAA sample, in contrast, in a similar experiment, exchanging the counterions in the same order resulted in a dramatic increase in the friction coefficient from 0.006 (Na^+) to 1.05 (Cu^{2+}) and 1.32 (Fe^{3+}). The pronounced changes in the friction properties of the PMAA brushes were attributed to the weak polyelectrolyte character of this polymer brush and the strong (inter and intrachain) ion-paring interactions that drive the collapse of these polymer films. For the strong PSPMA polyelectrolyte, in contrast, the multivalent Cu^{2+} and Fe^{3+} counterions are only relatively loosely bound, and only have a minor impact on the hydration, swelling and lubrication properties of the polymer brush film.

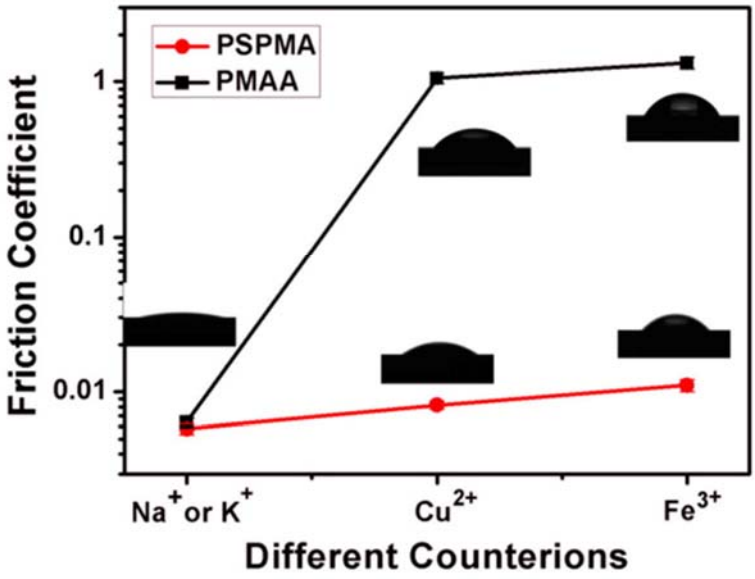

Figure 13: Friction coefficients and wettability (inserted images) of PMAA and PSPMA brushes in the presence of monovalent (Na^+ or K^+) counterions or coordinated with divalent Cu^{2+} and trivalent Fe^{3+} ions. Reprinted and adapted with permission from Ref.[59], Copyright (2013) American Chemical Society.

7. Stimuli-responsive polyelectrolyte brushes

The conformation and solution properties of polyelectrolytes are well-known to depend on environmental parameters such as ionic strength and pH.[41a] This applies to polyelectrolytes in solution, but even more so to surface-attached polyelectrolytes prepared via surface-initiated polymerization. In particular in cases were polyelectrolytes are tethered at short interchain distances with one chain end to the surface, strong interchain interactions can amplify effects of variations of, for example, solution pH and result in dramatic changes in the conformation of the polymer tethers (and concomitantly in the properties of these thin polymer films). Table 3 provides an overview of such stimuli-responsive polyelectrolyte brushes, which have been obtained via surface-initiated atom transfer radical polymerization. Yu et al. used neutron reflectivityand surface forces apparatus (SFA) experiments to study the structure of polystyrene sulfonate (PSS) brushes in the presence of mono-, di- and trivalent counterions.[29d] Figure 14 recapitulates some of the outcomes of these experiments. With Na^+ as the counterion, the results of the NR and SFA experiments agreed well with scaling theory, revealing two distinct regimes: the osmotic and salted brush regime. In the presence of trivalent Y^{3+} cations, the PSS brush abruptly shrinks due to the uptake of these cations (Figure 15). This process can be reversed by increasing the concentration of monovalent salt. Divalent cations, such as Mg^{2+}, Ca^{2+} and Ba^{2+}, were also found to significantly affect the structure of the PSS brushes. In case of these divalent cations, however, the specific response of the PSS brush was strongly dependent on the type of cation, which reflects the specific interactions between the divalent cations and the sulfonate groups.

Table 3: Overview of stimuli-responsive polyelectrolyte brushes prepared via SI-ATRP.

Polymer	**Substrate**	**Film thickness [nm]**	**Grafting density [chains/ nm^2]**	**Comment**	**Ref.**
PMETAC 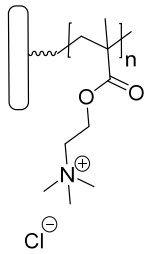	Gold surface	55 (water); 26 (1 M NaCl); 50 (dry)	N. A.	Counterion dependent modulation of swelling and wetting properties.	[63]
Q-PDMAEMA (via post-polymerization modification of PDMAEMA) 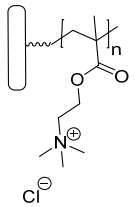	Gold covered silicon wafer	70 (dry); 180 (water); 145 (0.1 M NH_4PF_6); 145 (0.1 M Tf_2NLi)	N. A.	Counterion dependent swelling and collapse studied by electrochemical impedance spectroscopy.	[64]
PDMAEMA 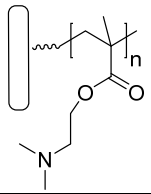	15.6 nm diameter silica nano-particle	28 (pH 5)	0.22	pH dependence of the interaction between the PDMAEMA brush and sodium dodecyl sulfate (SDS)	[65]
PDMAEMA-PS (via post-polymerization modification of PDMAEMA) 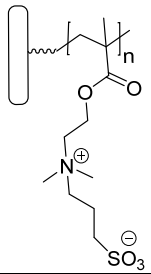	Si wafer	183.0 ± 5.6	0.45	Side chain functionality dependent hydration and swelling in humid vapor.	[66]

PDMAEMA-MeI (via post-polymerization modification of PDMAEMA) 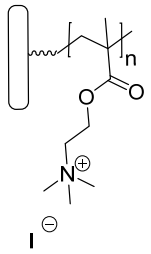	Si wafer	122.9 ± 0.1	0.45	Side chain functionality dependent hydration and swelling in humid vapor.	[66]
PDMAEMA-PrI (via post-polymerization modification of PDMAEMA) 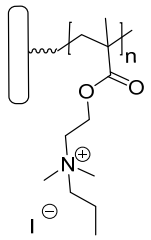	Si wafer	138.2 ± 1.0	0.45	Side chain functionality dependent hydration and swelling in humid vapor.	[66]
PDEA 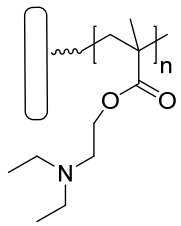	Single crystal Si block	16.1 (pD 10.86); 59.7 (pD 5.01)	N. A.	pH dependent hydration and swelling studied by simultaneous neutron reflectivity and in situ ATR-FTIR.	[67]
	Si particles (d = 120–840 nm)	Up to 35 (on d = 120 nm particle)	N. A.	Effect of substrate curvature on the SI-ATRP mediated polymer growth.	[68]
	silicon	13 and 27.6 (dry)	N. A.	pH dependent conformational changes probed with scanning force microscopy, neutron reflectometry, and single molecule force measurements.	[69]
PMAA 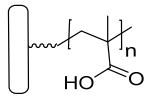	silicon	86.4 ± 16.6 (pH 3); 170.7 ± 47.6 (pH 12)	N. A.	pH dependent conformational changes probed with scanning force microscopy.	[69]

PAA		16 (dry); 16 → 26 (pH 2 → pH 10); 22 → 17 upon addition of NaCl; 24 → 20 upon addition of $CaCl_2$	N. A.	pH and ion strength dependent swelling.	[70]
	Mica	2.3 ± 0.7 to 17	0.04–0.49	Effect of pH, salt, grafting density on swelling.	[43c]
PVP-*b*-PAA 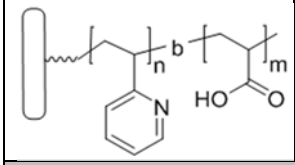	Si wafer	P2VP block: 5.2; PAA block: 1, 1.4 or 2.2	N. A.	pH dependent wetting properties and surface morphologies	[71]
PBpyClCl 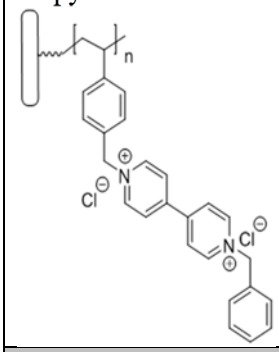	25 nm diameter silica nano particles	5 (dry, from XPS); 6.5 (wet, dynamic light scattering)	~ 0.5	Reversible reduction and oxidation upon exposure to UV light, respectively, air.	[72]
PSSNa 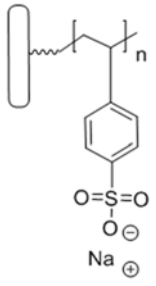	silicon wafer	12.6, 13.5	N. A.	Effect of multivalent counterions on brush structure.	[29c]
	silicon oxide, mica	24, 25 (silicon); 7 (mica)	0.1 (silicon); 0.025 (mica)	Brush structure in presence of multivalent counterions.	[29d]

PMAA + Azo-TMAB 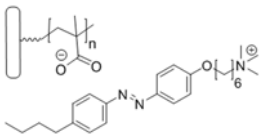	silicon wafer	24 ± 1 (PAA); 157 ± 4 (PAA + Azo-TMAB); 83 ± 2 (PAA); 340 ± 5 (PAA + Azo-TMAB)	0.4	Light induced changes of thickness and surface roughness.	[73]
PMMA-*b*-PMAA + Azo-TMAB 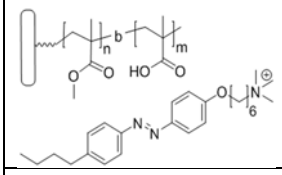	Si wafer	21–38 (PMMA-*b*-PMAA); 62–86 (PMMA-*b*-PMAA + Azo-TMAB)	0.4	Opto-mechanical scission of polymer chains.	[74]
PMAA-DR1 Ester 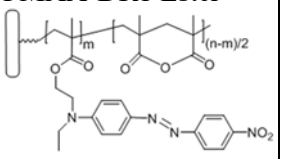		60, 140, 152	N. A.	Covalent bond scission and degrafting upon UV irradiation.	[75]

PDMAEMA = poly(2-dimethylaminoethyl methacrylate), PMETAC = poly([2-(methacryloyloxy)ethyl]-trimethylammonium chloride), PMAA = poly(methacrylic acid), PVP = poly(2-vinylpyridine), AzO-TMAB = Azobenzene containing trimethylammonium bromide surfactant, PMAA-DR1 ester = PMAA-disperse red ester, PSSNA = polystyrene sulfonic acid sodium salt, PBPYClCl = poly(*n*-benzyl-N`-(4-vinylbenzyl)-4,4`-bipyridium dichloride), PDEA = poly(2-(diethylamino)ethyl methacrylate), PDMAEMA-PS = poly(2-dimethylaminoethyl methacrylate) modified with propane sultone, PDMAEMA-PrI = poly(2-dimethylaminoethyl methacrylate) modified with pyropyl iodide, PDMAEMA-MeI = poly(2-dimethylaminoethyl methacrylate) modified with methyl iodide, PDMAEMA-Q = poly(2-dimethylaminoethyl methacrylate) modified with methyl iodide.

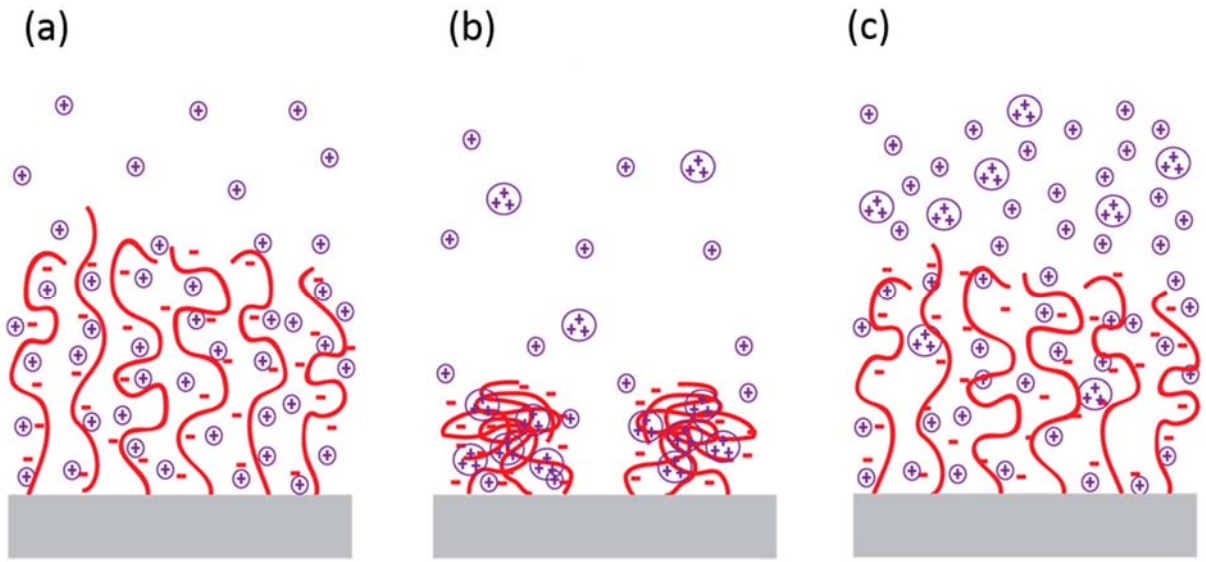

Figure 14: Schematic illustration of the structure of a PSS brush in the presence of different counterions. By variation of the external salt environment surrounding the end-tethered polyelectrolyte chains, a polyelectrolyte brush can transition from an extended brush structure (a) to a pinned micelle-like structure (b) and an extended brush again at high concentration of monovalent salt (c). Reprinted and adapted with permission from Ref.[29d], Copyright (2016) American Chemical Society.

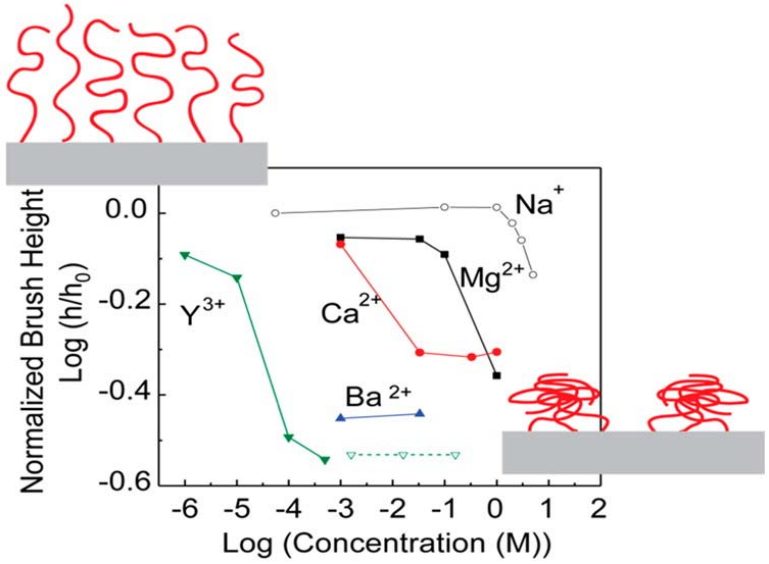

Figure 15: Normalized brush height h/h_0 measured by neutron reflectivity and plotted against the concentration of cations with different valencies, Na^+, Mg^{2+}, Ca^{2+}, Ba^{2+}, and Y^{3+}, on a log−log scale. The brush heights are normalized by the brush height of (1) the PSS brush in

D_2O for the data taken in $NaNO_3$ solutions, (2) the PSS brush in 3 mM $NaNO_3$ solutions for the data taken in $Mg(NO_3)_2$, $Ca(NO_3)_2$, and $Mg(NO_3)_2$ solutions, and (3) the PSS brush in 6 mM $NaNO_3$ solution for data taken in $Y(NO_3)_3$ solutions. Reprinted and adapted with permission with permission from Ref.[29d], Copyright (2016) American Chemical Society.

Moya et al. investigated the response of PMETAC brushes towards different electrolytes (NaCl and $MgSO_4$) using atomic force microscopy (AFM) and quartz crystal microbalance with dissipation (QCM-D) experiments.[63] The AFM cross-sectional profiles in Figure 16 illustrate the swelling of the PMETAC brushes in aqueous solution, the collapse of this film upon exposure to 1 M NaCl and the subsequent reversal of this collapse by exposing the film again to pure water. In the presence of $MgSO_4$ a very different behavior was observed. In this case, exchanging the solvent from water to 0.1 M $MgSO_4$ resulted in an irreversible collapse of the PMETAC brush, which retained its structure even after replacement in pure water. The collapsed PMETAC brushes, however, could be unlocked by exposure to a 1 M NaCl solution.

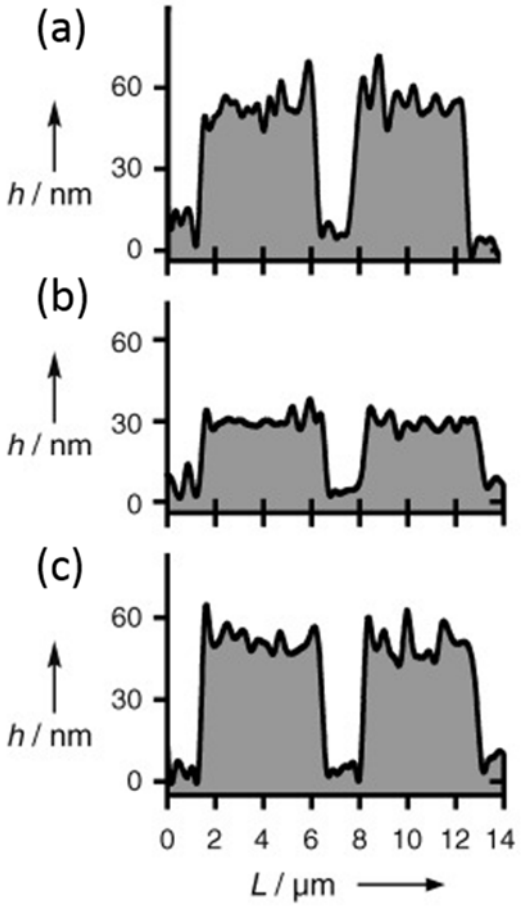

Figure 16: Cross-sectional AFM images of PMETAC brushes in (a) water, (b) 1 M NaCl and (c) in water after treatment with 1 M NaCl. Reprinted and adapted with permission from Ref.[63]

.

Along the same lines, also the influence of solution pH on the conformation of surface-grafted PMAA and PAA poly(acrylic acid) (PAA) brushes has been studied.[69-70] Figure 17 illustrates the pH dependent swelling of a PMAA brush. In acidic media (e.g., pH 3) the carboxylic acid side chain functional groups of the PMAA tethers are protonated and the brush collapses to a height of 86.4 nm. An increase in pH of the surrounding solution to pH 12 results in deprotonation of the carboxylic acid moieties and in repulsive electrostatic interactions that lead to a swelling of the polymer brush to a thickness of ~ 170 nm.

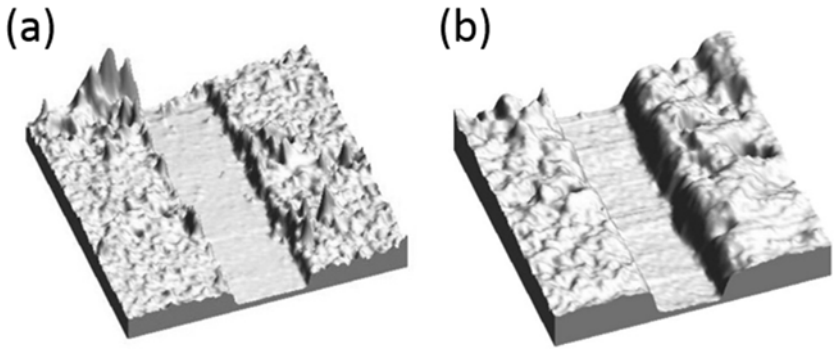

Figure 17: AFM images of (a) a collapsed dense PMAA bush in dilute H_2SO_4 (pH 3) (the trough is a scratch down to the bare silicon surface); (b) The same dense polymer brush swollen in dilute NaOH (pH 12). Reprinted and adapted with permission from Ref.[69].

Santer et al. explored the photosensitive azobenzene moiety to modulate the structure and properties of surface grafted polymer brush films.[73-75] In a first example, azobenzene groups were covalently attached to the side chains of poly(methacrylic acid) brushes prepared by surface-initiated polymerization.[75] While irradiation with homogeneous irradiation had no effect on the structure of the brush, irradiation with a UV interference pattern resulted in chain scission and the irreversible formation of surface relief gratings.[75] Similar observations were made when PMMA-*b*-PMAA diblock copolymer brush films were studied, which incorporated a cationic azobenzene surfactant via electrostatic interactions in the PMAA block.[74] In a final example, atomic force microscopy was used to study light-induced changes in the film thickness and surface roughness of photosensitive polymer brushes containing a cationic azobenzene cationic surfactant (Figure 18).[73] The observed changes in film thickness and surface roughness were attributed due to the differences in polarity of the azobenzene moieties in the cis and in the trans state. It was proposed that the azobenzene surfactants formed aggregates in the brush while in their trans form. Upon irradiation, the azobenzene surfactant isomerizes into the more hydrophilic cis state. Since the azobenzene moieties are more hydrophilic in the cis state, the aggregates in the brush are disrupted, and the polymer brush contracts. Subsequent irradiation with blue light resulted in reversal of this process.

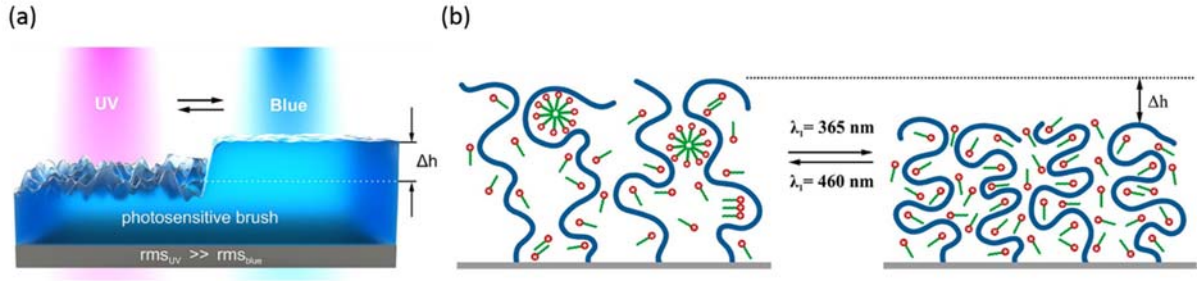

Figure 18: Schematic illustration of the light-induced changes in film thickness and surface roughness of azobenzene surfactant incorporating poly(methacrylic acid) brushes. Reprinted and adapted with permission from Ref.[73], Copyright (2013) American Chemical Society.

8. Summary

Polyelectrolyte brushes are of great importance to a variety of applications, including colloidal stabilization, drug and therapeutic delivery, antifouling, and lubrication.[2, 4b, 5-7, 11b, 47d, 49-50, 53] The stimuli-responsiveness of these systems has further inspired numerous studies towards the development of functional brush surfaces. Many of the unique properties of polyelectrolyte brushes are due to the specific interactions that act in and on these surface-tethered polymer films, including solvent structure effects, hydrophobic forces, electrostatic interactions, and specific ion interactions. Understanding the effects of these specific interactions on under various solution conditions is therefore of significant importance for many applications involving functional polyelectrolyte brushes.

In this review, we have provided an overview of the current theoretical framework that is used to describe the structure and properties of polyelectrolyte brushes, as well as two important experimental techniques that are widely used to study and characterize these polymer brushes, viz. SFA and AFM. Moreover, we summarized recent progress of utilizing polyelectrolyte brush functionalized surfaces in anti-fouling, boundary lubrication, and stimuli-response applications. With unique functionalities and specific interactions with various environment stimulations, polyelectrolyte brushes have gained popularity in the realm of functional soft interfaces. The rapid development of surface-initiated polymerization techniques opens new avenues in functional polyelectrolyte brushes. Along with creating polyelectrolyte brush surfaces for novel applications, future work on polyelectrolyte brushes should also aim at developing suitable techniques for the characterization of the structure and functionalities of polyelectrolyte brushes at the molecular scale, especially in real-time. Although this review mainly focuses on strong polyelectrolyte brushes, there remains a lot to be done in the area of weak (annealed) polyelectrolyte brushes considering their responsive nature to the surrounding solution environment.

Acknowledgement

This work was supported by a start-up grant of NTU, M4082049.070, and Singapore Ministry of Education Academic Research Fund Tier 1 2017-T1-002-092 (XX and JY). This material is based upon work supported by the National Science Foundation under Grants No. NSF-CMMI-1562876 (XX) and NSF-CMMI-1161475 (MR). This research has been financially supported by the Swiss National Science Foundation (SNSF) and by Innosuisse.

References

[1] a) P. G. Degennes, *Macromolecules* **1980**, *13*, 1069-1075; b) S. T. Milner, T. A. Witten and M. E. Cates, *Macromolecules* **1988**, *21*, 2610-2619; c) M. Muthukumar and J. S. Ho, *Macromolecules* **1989**, *22*, 965-973.
[2] P. Pincus, *Macromolecules* **1991**, *24*, 2912-2919.
[3] a) D. H. Napper, *Polymeric stabilization of colloidal dispersions*, Academic Press, London ; New York, **1983**, p. xvi, 428 p; b) J. Klein, *Annu. Rev. Mater. Sci.* **1996**, *26*, 581; c) O. Al-Jaf, A. Alswieleh, S. P. Armes and G. J. Leggett, *Soft Matter* **2017**, *13*, 2075-2084; d) X. Banquy, J. Burdynska, D. W. Lee, K. Matyjaszewski and J. Israelachvili, *Journal of the American Chemical Society* **2014**, *136*, 6199-6202.
[4] a) M. Kobayashi, Y. Terayama, H. Yamaguchi, M. Terada, D. Murakami, K. Ishihara and A. Takahara, *Langmuir* **2012**, *28*, 7212-7222; b) U. Raviv, S. Giasson, N. Kampf, J.-F. Gohy, R. Jerome and J. Klein, *Nature* **2003**, *425*, 163-165.
[5] a) N. Welsch, Y. Lu, J. Dzubiella and M. Ballauff, *Polymer* **2013**, *54*, 2835-2849; b) E. Karzbrun, A. M. Tayar, V. Noireaux and R. H. Bar-Ziv, *Science* **2014**, *345*, 829.
[6] R. Fan, O. Vermesh, A. Srivastava, B. K. H. Yen, L. Qin, H. Ahmad, G. A. Kwong, C.-C. Liu, J. Gould, L. Hood and J. R. Heath, *Nature Biotechnology* **2008**, *26*, 1373.
[7] T. G. Drummond, M. G. Hill and J. K. Barton, *Nature Biotechnology* **2003**, *21*, 1192.
[8] M. E. Welch, N. L. Ritzert, H. Chen, N. L. Smith, M. E. Tague, Y. Xu, B. A. Baird, H. D. Abruna and C. K. Ober, *J Am Chem Soc* **2014**, *136*, 1879-1883.
[9] D. Bracha, E. Karzbrun, G. Shemer, P. A. Pincus and R. H. Bar-Ziv, *Proceedings of the National Academy of Sciences* **2013**, *110*, 4534.
[10] a) S. Jahn, J. Seror and J. Klein, *Annual Review of Biomedical Engineering* **2016**, *18*, 235-258; b) B. Zappone, K. J. Rosenberg and J. Israelachvili, *Tribology Letters* **2007**, *26*, 191-201; c) S. Lee and N. D. Spencer, *Science* **2008**, *319*, 575-576.
[11] a) E. B. Zhulina and M. Rubinstein, *Macromolecules* **2014**, *47*, 5825-5838; b) M. Chen, W. H. Briscoe, S. P. Armes and J. Klein, *Science* **2009**, *323*, 1698-1701.
[12] W.-L. Chen, R. Cordero, H. Tran and C. K. Ober, *Macromolecules* **2017**, *50*, 4089-4113.
[13] a) T. Wu, P. Gong, I. Szleifer, P. Vlcek, V. Subr and J. Genzer, *Macromolecules* **2007**, *40*, 8756; b) P. Gong, T. Wu, J. Genzer and I. Szleifer, *Macromolecules* **2007**, *40*, 8765.
[14] a) R. Israels, F. A. M. Leermakers, G. J. Fleer and E. B. Zhulina, *Macromolecules* **1994**, *27*, 3249-3261; b) O. V. Borisov, T. M. Birshtein and E. B. Zhulina, *Journal de Physique II* **1991**, *1*, 521-526; c) O. V. Borisov, E. B. Zhulina and T. M. Birshtein, *Macromolecules* **1994**, *27*, 4795-4803.
[15] O. Azzaroni, S. E. Moya, A. A. Brown, Z. Zheng, E. Donath and W. T. S. Huck, *Advanced Functional Materials* **2006**, *16*, 1037-1042.
[16] Y. Zhu, F. Zhang, D. Wang, X. F. Pei, W. Zhang and J. Jin, *Journal of Materials Chemistry A* **2013**, *1*, 5758-5765.
[17] J. Yang, H. Chen, S. Xiao, M. Shen, F. Chen, P. Fan, M. Zhong and J. Zheng, *Langmuir* **2015**, *31*, 9125-9133.
[18] R. Toomey and M. Tirrell, *Annual Review of Physical Chemistry* **2008**, *59*, 493-517.
[19] P. J. Flory, *Principles of polymer chemistry*, Cornell University Press, Ithaca,, **1953**, p. 672 p.
[20] P. G. d. Gennes, *Scaling concepts in polymer physics*, Cornell University Press, Ithaca, N.Y., **1979**, p. 324 p.

[21] A. Halperin, M. Tirrell and T. P. Lodge, *Advances in Polymer Science* **1992**, *100*, 31-71.
[22] H. Schiessel and P. Pincus, *Macromolecules* **1998**, *31*, 7953.
[23] a) E. B. Zhulina, J. K. Wolterink and O. V. Borisov, *Macromolecules* **2000**, *33*, 4945-4953; b) O. V. Borisov and E. B. Zhulina, *Journal De Physique Ii* **1997**, *7*, 449-458; c) E. B. Zhulina, O. V. Borisov and T. M. Birshtein, *Journal De Physique Ii* **1992**, *2*, 63-74.
[24] a) F. Li, M. Balastre, P. Schorr, J. F. Argillier, J. Yang, J. W. Mays and M. Tirrell, *Langmuir* **2006**, *22*, 4084-4091; b) M. Balastre, F. Li, P. Schorr, J. Yang, J. W. Mays and M. V. Tirrell, *Macromolecules* **2002**, *35*, 9480-9486; c) H. Ahrens, S. Forster and C. A. Helm, *Physical Review Letters* **1998**, *81*, 4172-4175.
[25] P. Guenoun, J. F. Argillier and M. Tirrell, *Comptes Rendus De L Academie Des Sciences Serie Iv Physique Astrophysique* **2000**, *1*, 1163-1169.
[26] Y. Tran, P. Auroy and L. T. Lee, *Macromolecules* **1999**, *32*, 8952-8964.
[27] a) G. S. Manning, *The Journal of Chemical Physics* **1969**, *51*, 924-933; b) P. Kaewsaiha, K. Matsumoto and H. Matsuoka, *Langmuir* **2007**, *23*, 20-24.
[28] a) Y. Mei, M. Hoffmann, M. Ballauff and A. Jusufi, *Physical Review E* **2008**, *77*, 031805; b) Y. Mei, K. Lauterbach, M. Hoffmann, O. V. Borisov, M. Ballauff and A. Jusufi, *Physical Review Letters* **2006**, *97*, 158301.
[29] a) R. Farina, N. Laugel, P. Pincus and M. Tirrell, *Soft Matter* **2013**, *9*, 10458; b) R. Farina, N. Laugel, J. Yu and M. Tirrell, *The Journal of Physical Chemistry C* **2015**, *119*, 14805-14814; c) J. Yu, J. Mao, G. Yuan, S. Satija, W. Chen and M. Tirrell, *Polymer* **2016**, *98*, 448-453; d) J. Yu, J. Mao, G. Yuan, S. Satija, Z. Jiang, W. Chen and M. Tirrell, *Macromolecules* **2016**, *49*, 5609-5617.
[30] B. Brettmann, P. Pincus and M. Tirrell, *Macromolecules* **2017**, *50*, 1225-1235.
[31] L. Liu, P. A. Pincus and C. Hyeon, *Macromolecules* **2017**, *50*, 1579-1588.
[32] N. E. Jackson, B. K. Brettmann, V. Vishwanath, M. Tirrell and J. J. de Pablo, *ACS Macro Letters* **2017**, *6*, 155-160.
[33] J. Yu, N. E. Jackson, X. Xu, B. K. Brettmann, M. Ruths, J. J. de Pablo and M. Tirrell, *Science Advances* **2017**, *3*.
[34] a) D. Bracha and R. H. Bar-Ziv, *J Am Chem Soc* **2014**, *136*, 4945-4953; b) W. H. Wang, L. Li, K. Henzler, Y. Lu, J. Y. Wang, H. Y. Han, Y. C. Tian, Y. W. Wang, Z. M. Zhou, G. Lotze, T. Narayanan, M. Ballauff and X. H. Guo, *Biomacromolecules* **2017**, *18*, 1574-1581; c) Y. Lu and M. Ballauff, *Progress in Polymer Science* **2016**, *59*, 86-104; d) Q. Q. Cao and M. Bachmann, *Soft Matter* **2013**, *9*, 5087-5098.
[35] a) M. Tirrell, S. Patel and G. Hadziioannou, *Proceedings of the National Academy of Sciences* **1987**, *84*, 4725-4728; b) T. W. Kelley, P. a. Schorr, K. D. Johnson, M. Tirrell and C. D. Frisbie, *Macromolecules* **1998**, *31*, 4297-4300.
[36] N. Iuster, O. Tairy, M. J. Driver, S. P. Armes and J. Klein, *Macromolecules* **2017**, *50*, 7361-7371.
[37] P. M. Claesson, T. Ederth, V. Bergeron and M. W. Rutland, *Advances in Colloid and Interface Science* **1996**, *67*, 119-183.
[38] a) N. Kampf, J. F. Gohy, R. Jérôme and J. Klein, *Journal of Polymer Science Part B: Polymer Physics* **2004**, *43*, 193-204; b) M. Benz, N. Chen and J. Israelachvili, *Journal of Biomedical Materials Research Part A* **2004**, *71A*, 6-15; c) U. Raviv, S. Giasson, N. Kampf, J.-F. Gohy, R. Jérôme and J. Klein, *Langmuir* **2008**, *24*, 8678-8687; d) S. Giasson, J.-M. Lagleize, J. Rodríguez-Hernández and C. Drummond, *Langmuir* **2013**, *29*, 12936-12949; e) J. Yu, X. Banquy, G. W. Greene, D. D. Lowrey and J. N. Israelachvili, *Langmuir* **2012**, *28*, 2244-2250; f) D. W. Lee, X. Banquy and J. N. Israelachvili, *Proceedings of the National Academy of Sciences of the United States of America* **2013**, *110*, E567-E574.
[39] L. Ma, A. Gaisinskaya-Kipnis, N. Kampf and J. Klein, *Nature Communications* **2015**, *6*, 6060.
[40] E. Eiser and J. Klein, *Macromolecules* **2007**, *40*, 8455-8463.
[41] a) A. B. Lowe and C. L. McCormick, *Chemical Reviews* **2002**, *102*, 4177-4190; b) M. Kobayashi and A. Takahara, *The Chemical Record* **2010**, *10*, 208-216; c) D. Wang and T. P. Russell, *Macromolecules* **2018**, *51*, 3-24.

[42] a) T. Farhan, O. Azzaroni and W. T. S. Huck, *Soft Matter* **2005**, *1*, 66-66; b) S. Gupta, M. Agrawal, P. Uhlmann and M. Stamm, *American Chemical Society* (New Orleans, LA) **2008**, pp. 600-602; c) Z. Liu, J. Liu, H. Hu, B. Yu, M. Chen and F. Zhou, *Physical Chemistry Chemical Physics* **2008**, *10*, 7180-7185; d) I. Zalakain, N. Politakos, J. A. Ramos, A. Saralegi, H. Etxeberria, I. Mondragon, M. A. Corcuera and A. Eceiza, *European Polymer Journal* **2013**, *49*, 2120-2127.
[43] a) K. N. Witte, J. Hur, W. Sun, S. Kim and Y.-Y. Won, *Macromolecules* **2008**, *41*, 8960-8963; b) J. Hur, K. N. Witte, W. Sun and Y.-Y. Won, *Langmuir* **2010**, *26*, 2021-2034; c) B. Lego, W. G. Skene and S. Giasson, *Macromolecules* **2010**, *43*, 4384-4393; d) J. D. Willott, T. J. Murdoch, G. B. Webber and E. J. Wanless, *Macromolecules* **2016**, *49*, 2327-2338; e) M. Raftari, Z. J. Zhang, S. R. Carter, G. J. Leggett and M. Geoghegan, *Tribology Letters* **2017**, *66*, 11.
[44] A. Drechsler, M. M. Elmahdy, P. Uhlmann and M. Stamm, *Langmuir* **2018**, *34*, 4739-4749.
[45] a) Z. Zhang, A. J. Morse, S. P. Armes, A. L. Lewis, M. Geoghegan and G. J. Leggett, *Langmuir* **2013**, *29*, 10684-10692; b) Z. Zhang, M. Moxey, A. Alswieleh, A. J. Morse, A. L. Lewis, M. Geoghegan and G. J. Leggett, *Langmuir* **2016**, *32*, 5048-5057.
[46] Y. Yu, M. Cirelli, B. D. Kieviet, E. S. Kooij, G. J. Vancso and S. de Beer, *Polymer* **2016**, *102*, 372-378.
[47] a) H. Ma, J. Hyun, P. Stiller and A. Chilkoti, *Advanced Materials* **2004**, *16*, 338-341; b) A. Hucknall, S. Rangarajan and A. Chilkoti, *Advanced Materials* **2009**, *21*, 2441-2446; c) X. Fan, L. Lin, J. L. Dalsin and P. B. Messersmith, *Journal of the American Chemical Society* **2005**, *127*, 15843-15847; d) X. Fan, L. Lin and P. B. Messersmith, *Biomacromolecules* **2006**, *7*, 2443-2448; e) J. E. Raynor, J. R. Capadona, D. M. Collard, T. A. Petrie and A. J. García, *Biointerphases* **2009**, *4*, FA3-FA16; f) F. J. Xu, J. P. Zhao, E. T. Kang, K. G. Neoh and J. Li, *Langmuir* **2007**, *23*, 8585-8592; g) W. J. Yang, T. Cai, K.-G. Neoh, E.-T. Kang, S. L.-M. Teo and D. Rittschof, *Biomacromolecules* **2013**, *14*, 2041-2051; h) S. Tugulu and H.-A. Klok, *Biomacromolecules* **2008**, *9*, 906-912; i) T. D. Michl, C. Giles, P. Mocny, K. Futrega, M. R. Doran, H.-A. Klok, H. J. Griesser and B. R. Coad, *Biointerphases* **2017**, *12*, 05G602; j) L. Lavanant, B. Pullin, A. Hubbell Jeffrey and H. A. Klok, *Macromolecular Bioscience* **2009**, *10*, 101-108.
[48] a) J. Ladd, Z. Zhang, S. Chen, J. C. Hower and S. Jiang, *Biomacromolecules* **2008**, *9*, 1357-1361; b) T. Tah and M. T. Bernards, *Colloids and Surfaces B: Biointerfaces* **2012**, *93*, 195-201.
[49] Z. Zhang, T. Chao, S. Chen and S. Jiang, *Langmuir* **2006**, *22*, 10072-10077.
[50] M. T. Bernards, G. Cheng, Z. Zhang, S. Chen and S. Jiang, *Macromolecules* **2008**, *41*, 4216-4219.
[51] Y. Higaki, J. Nishida, A. Takenaka, R. Yoshimatsu, M. Kobayashi and A. Takahara, *Polymer Journal* **2015**, *47*, 811.
[52] D. Pranantyo, L. Q. Xu, K.-G. Neoh, E.-T. Kang, Y. X. Ng and S. L.-M. Teo, *Biomacromolecules* **2015**, *16*, 723-732.
[53] A. M. Brzozowska, F. J. Parra-Velandia, R. Quintana, Z. Xiaoying, S. S. C. Lee, L. Chin-Sing, D. Jańczewski, S. L. M. Teo and J. G. Vancso, *Langmuir* **2014**, *30*, 9165-9175.
[54] H. Chen, J. Yang, S. Xiao, R. Hu, S. M. Bhaway, B. D. Vogt, M. Zhang, Q. Chen, J. Ma, Y. Chang, L. Li and J. Zheng, *Acta Biomaterialia* **2016**, *40*, 62-69.
[55] P. Mocny and H.-A. Klok, *Molecular Systems Design & Engineering* **2016**, *1*, 141-154.
[56] B. Li, B. Yu, X.-l. Wang, F. Guo and F. Zhou, *Chinese Journal of Polymer Science* **2015**, *33*, 163-172.
[57] B. Wu, X. Wang, J. Yang, Z. Hua, K. Tian, R. Kou, J. Zhang, S. Ye, Y. Luo, V. S. J. Craig, G. Zhang and G. Liu, *Science Advances* **2016**, *2*.
[58] M. Kobayashi, M. Terada and A. Takahara, *Faraday Discussions* **2012**, *156*, 403-412.
[59] Q. Wei, M. Cai, F. Zhou and W. Liu, *Macromolecules* **2013**, *46*, 9368-9379.
[60] M. Chen, W. H. Briscoe, S. P. Armes, H. Cohen and J. Klein, *European Polymer Journal* **2011**, *47*, 511-523.
[61] M. Kobayashi, H. Tanaka, M. Minn, J. Sugimura and A. Takahara, *ACS Applied Materials & Interfaces* **2014**, *6*, 20365-20371.
[62] X. Pei, Y. Xia, W. Liu, B. Yu and J. Hao, *Journal of Polymer Science Part A: Polymer Chemistry* **2008**, *46*, 7225-7237.

[63] S. Moya, O. Azzaroni, T. Farhan, L. Osborne Vicky and T. S. Huck Wilhelm, *Angewandte Chemie International Edition* **2005**, *44*, 4578-4581.
[64] F. Zhou, H. Hu, B. Yu, V. L. Osborne, W. T. S. Huck and W. Liu, *Analytical Chemistry* **2007**, *79*, 176-182.
[65] J. K. Riley, J. An and R. D. Tilton, *Langmuir* **2015**, *31*, 13680-13689.
[66] C. J. Galvin, M. D. Dimitriou, S. K. Satija and J. Genzer, *Journal of the American Chemical Society* **2014**, *136*, 12737-12745.
[67] P. D. Topham, A. Glidle, D. T. W. Toolan, M. P. Weir, M. W. A. Skoda, R. Barker and J. R. Howse, *Langmuir* **2013**, *29*, 6068-6076.
[68] B. T. Cheesman, A. J. G. Neilson, J. D. Willott, G. B. Webber, S. Edmondson and E. J. Wanless, *Langmuir* **2013**, *29*, 6131-6140.
[69] A. J. Ryan, C. J. Crook, J. R. Howse, P. Topham, M. Geoghegan, S. J. Martin, A. J. Parnell, L. Ruiz-Pérez and R. A. L. Jones, *Journal of Macromolecular Science, Part B* **2005**, *44*, 1103-1121.
[70] N. Ayres, S. G. Boyes and W. J. Brittain, *Langmuir* **2007**, *23*, 182-189.
[71] K. Yu, H. Wang, L. Xue and Y. Han, *Langmuir* **2007**, *23*, 1443-1452.
[72] F. J. Xu, F. B. Su, S. B. Deng and W. T. Yang, *Macromolecules* **2010**, *43*, 2630-2633.
[73] A. Kopyshev, C. J. Galvin, R. R. Patil, J. Genzer, N. Lomadze, D. Feldmann, J. Zakrevski and S. Santer, *ACS Applied Materials & Interfaces* **2016**, *8*, 19175-19184.
[74] A. Kopyshev, C. J. Galvin, J. Genzer, N. Lomadze and S. Santer, *Langmuir* **2013**, *29*, 13967-13974.
[75] N. Lomadze, A. Kopyshev, J. Rühe and S. Santer, *Macromolecules* **2011**, *44*, 7372-7377.